

Donor-Acceptor Boron-Ketoiminate Complexes With Pendent *N*-Heterocyclic Arms: Switched-On Luminescence Through *N*-Heterocycle Methylation

*Issiah B. Lozada,^a Robert J. Ortiz,^a Jason D. Braun,^a J. A. Gareth Williams^b and David
E. Herbert^{a*}*

^aDepartment of Chemistry and the Manitoba Institute for Materials, University of
Manitoba, 144 Dysart Road, Winnipeg, Manitoba, R3T 2N2, Canada

^bDepartment of Chemistry, Durham University, Durham, DH1 3LE, UK

*david.herbert@umanitoba.ca

ABSTRACT

A series of intramolecular, donor-stabilized BF₂ complexes supported by phenanthridinyl-decorated, β-ketoiminate chelating ligand scaffolds is described, along with their characterization by spectroscopy and X-ray diffraction. In solution, the relative orientation of the pendent phenanthridinyl arm is fixed despite not coordinating to the boron center, and a well-resolved through-space interaction between a phenanthridinyl C-H and a single fluorine atom can be observed by ¹⁹F-¹H NOE NMR spectroscopy. The neutral compounds are nonetheless only weakly luminescent in fluid solution, ascribed to non-radiative decay pathways enabled by rotation of the *N*-heterocyclic unit. Methylation of the phenanthridinyl nitrogen restricts this rotation, “switching on” comparably strong emission in solution. Modelling by density functional theory (DFT) and time-dependent DFT (TDDFT) indicates that the character of the lowest energy excitations changes upon methylation, with shallow calculated potential energy surfaces of the neutral complexes consistent with their lack of significant radiative decay.

Introduction

Intramolecular donor-stabilized BF₂ complexes, including derivatives of the highly popular 4,4-difluoro-4-bora-3a,4a-diaza-*s*-indacenes (BODIPYs; **A**, Figure 1) and related diazaborinines, exhibit rich photophysical and electronic properties. Many are intensely fluorescent, and tunable across much of the visible spectrum and into the near-infrared. Accordingly, they have found use in a wide range of applications from photosensitization¹ to optoelectronics,² as stimuli-responsive materials,³ and in biological applications.⁴⁻⁶ A significant amount of effort has been put into developing chemical routes to modify the chromophoric core of BODIPYs, both through their primary synthesis⁷ and via postfunctionalization,⁸ enabling the fine-tuning and improvement of specific properties that can be tailored for bespoke applications. Beyond BODIPYs, other classes of difluoroboron-stabilized chromophores have also been developed that attempt to conserve the desirable characteristics of BODIPY dyes while addressing some of the drawbacks. These include diazaborinines (β -diiminates; **B**),⁹⁻¹¹ dioxaborinines (β -diketonates; **C**)^{12,13} and asymmetric azaoxaborinines (β -ketoiminates; **D**, **E**).

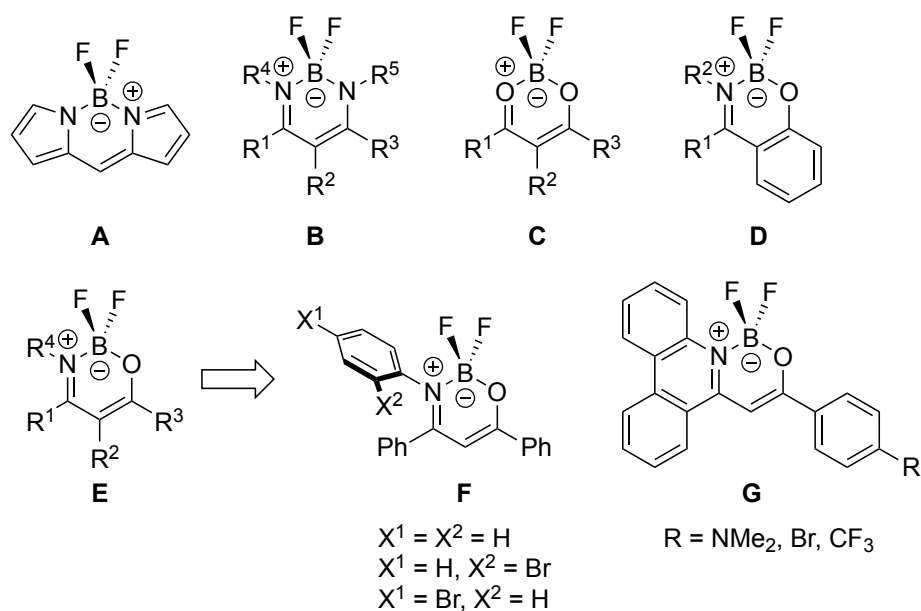


Figure 1. Selected examples of intramolecular donor-stabilized BF_2 -chelates.

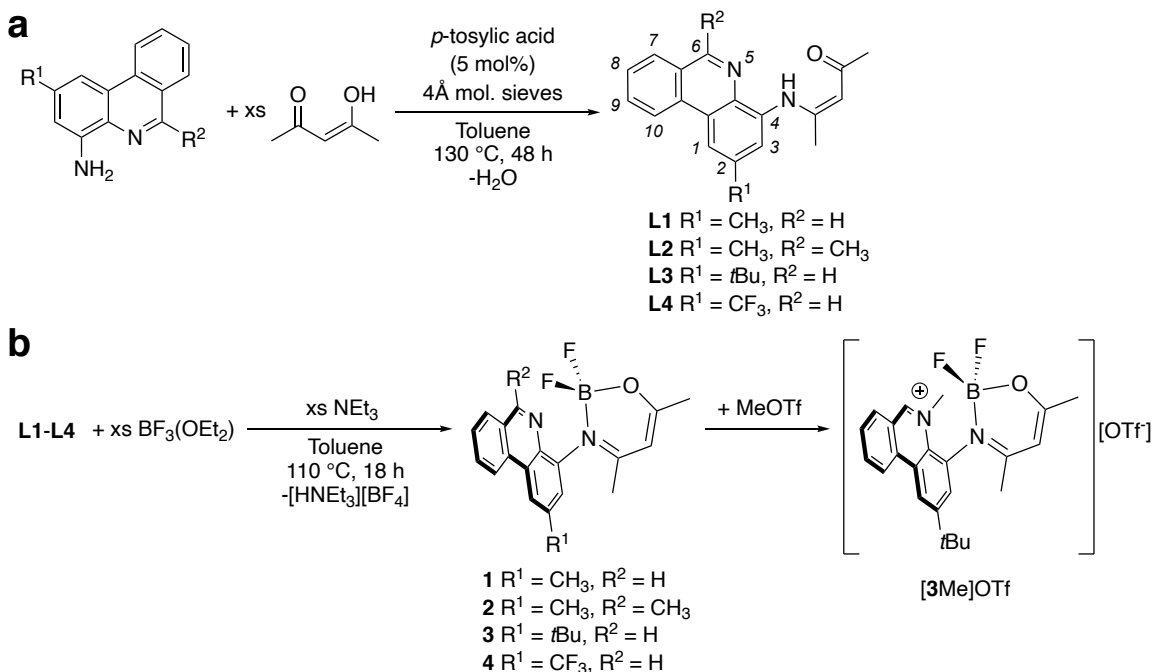
Diaza- (**B**) and dioxaborinines (**C**) represent the two most studied classes of six-membered difluoroboron-containing heterocycles. In comparison, asymmetric azaoxaborinine analogues containing an $\text{N}^{\ominus}\text{O}$ -bound BF_2 motif (**E-G**) represent an emerging class of emissive difluoroboron complexes. While these compounds have a longer history in photocycloaddition reactions with aryl alkenes,¹⁴⁻¹⁶ the potential of these compounds in materials chemistry is now being realized. In this context, Gardinier and coworkers have investigated the impact on the electronic structure of difluoroboron complexes upon mono- and di-substitution of the oxygen-donor atoms with nitrogen, revealing the intermediacy of the difluoroboron β -ketominates as electron donors and acceptors compared to symmetric $\text{O}^{\ominus}\text{O}$ or $\text{N}^{\ominus}\text{N}$ chelates.⁹ Of the various $\text{N}^{\ominus}\text{O}$ -containing difluoroboron complexes that have been reported,^{9,17-19} considerable attention has been dedicated to the boranil analogues (**D**), first reported by Ziesel and co-workers,²⁰ from both application²¹⁻²³ and theoretical²⁴ points of view.

We recently reported the construction of monoanionic 4-(4-enamino-2-*R*-phenanthridinyl)-3-penten-2-one ($R = t\text{Bu}, \text{CF}_3$) ligand scaffolds bearing benzannulated phenanthridine (3,4-benzoquinoline) units.²⁵ The incorporation of phenanthridine into β -ketoimine ligand-supported BF_2 adducts has been previously accomplished in the form of (*Z*)-6-(2-((difluoroboryl)oxy)-2-phenylvinyl)phenanthridines¹⁹ (**G**). While most difluoroboron β -ketoiminates are at best only weakly emissive in solution,^{9,18} these complexes show enhanced emission quantum yields, particularly when a strongly electron-releasing NMe_2 substituent is attached in the *para*-position of the phenyl fragment. Encouraged by these results and intrigued by the potential effects on the electronic structure and photophysical properties of our ligand platform, we prepared four new difluoroboron complexes supported by deprotonated 4-(4-enamino-2-*R*-phenanthridinyl)-3-penten-2-one ligands. While their neutral BF_2 chelates are only weakly emissive in fluid solution, methylation of the pendent phenanthridinyl arm was found to significantly boost emission from the resulting cation.

RESULTS AND DISCUSSION

Ligand and complex synthesis. To prepare proligands **L1** and **L2**, we followed the published procedure for the synthesis of **L3** and **L4**.²⁵ Briefly, for the new compounds described here, the acid-catalyzed condensation of 2-methyl²⁶ and 2,6-dimethyl-substituted 4-aminophenanthridines²⁷ with acetylacetone (Scheme 1a) was used to construct the adjoining C-N bond. Inclusion of a CH_3 at the 2- and/or 6-positions of the phenanthridinyl moiety did not significantly impact the overall reaction and the two new proligands were isolated in similar yields (64-72%) and with sufficient purity to be used without further

purification. All four proligands exhibit similar solution NMR and IR spectra and are predominantly in the keto-enamine tautomeric form. The presence of electron-releasing substituents in the 2-position (CH₃, **L1**; *t*Bu, **L3**) shifts the C=O stretching and N–H bending modes to lower energy in **L1** and **L3** compared with the electron-withdrawing CF₃-substituent in **L4** ($\nu_{\text{C=O}}$: 1617, 1617 and 1634 cm⁻¹ and $\nu_{\text{N-H}}$: 1569, 1570, and 1579 cm⁻¹ for **L1**, **L3** and **L4** respectively).



Scheme 1. Synthesis of proligands (**L1-L4**) and their boron difluoride complexes (**1-4**). The IUPAC numbering system for phenanthridines is illustrated in italics for the proligands.

L1-L4 were reacted with boron trifluoride diethyl etherate in the presence of excess base (NEt₃) to install a BF₂ unit (Scheme 1b). Substitution in the 2-position of phenanthridine (R¹) had no significant influence on the overall progress of the reaction, and compounds **1**, **3** and **4** were isolable as brown or orange solids in high yields (72-86%).

A lower yield was observed for **2** (38%), possibly attributable to the presence of a more sterically demanding CH₃ at the 6-position of the phenanthridinyl arm (R²). The isolated compounds were found to be stable to air and ambient moisture, in solution and the solid-state, and to protic solvents such as alcohols. Both solution (NMR) and solid-state (ATR-IR) spectra of the complexes are consistent with ligand deprotonation and binding to boron. For example, the resonance attributed to the enamine proton in the ¹H NMR spectra (δ_{NH}/ppm : **L1**, 13.53; **L2**, 13.61; **L3**, 13.44; **L4**, 13.72) and the N–H bending mode in the IR ($\nu_{N-H, \text{ bend}}/\text{cm}^{-1}$: **L1**, 1569; **L2**, 1569; **L3**, 1570; **L4**, 1579) are both absent in the spectra of the complexes. In addition, the *CH* resonance of the methine group of the ketoenamine subunit is shifted downfield by ~0.3 ppm. A comparably more minor shift is observed for the ¹H resonance attributed to the *CH* unit in the 6-position of phenanthridine, with an average upfield shift of ~0.09 ppm. Our previous studies on coordination complexes supported by phenanthridine-based ligands typically saw larger shifts in the ¹H resonance of the C₆H (using the IUPAC numbering highlighted in Scheme 1) upon binding to Lewis acids such as transition metals, with the shift being dependent on the metal.²⁸ Indeed, Pt(II) complexes of **L3** and **L4** exhibit a more pronounced downfield shift on the C₆H resonance of ~0.7 ppm.²⁵ The ¹H NMR spectroscopy therefore implies that the phenanthridinyl unit does not associate significantly with the boron center in solution. High-resolution mass spectrometry of **1-4** supports their formulation as 1:1 ligand-BF₂ complexes.

Despite the lack of phenanthridine coordination, no dynamic processes associated, for example, with rotation about the C₄–N bond axis are observed at room temperature by solution NMR spectroscopy. ¹⁹F NMR spectra of **1-4** exhibit two distinct doublet-of-quartet resonances due to the inequivalence of the fluorine nuclei (Figure 2a). A doublet-

of-doublets is accordingly observed in the ^{11}B NMR spectra, consistent with a rigid BF_2 unit. These signals are quite sharp and well-resolved compared to the broad resonances for $\text{BF}_3(\text{OEt}_2)$.²⁹ Most *N*-aryl-substituted difluoroboron ketoiminates, in comparison, exhibit a more symmetric boron environment with a single quartet resonance in the ^{19}F NMR and a triplet resonance in the ^{11}B NMR appearing at ~ 0 ppm.⁹ Increasing the steric congestion close to boron through inclusion of substituents *ortho* to the nitrogen donor (e.g., when $\text{X}^2 = \text{Br}$ in **F**, Figure 1), however, or any introduction of asymmetry at the *N*-aryl substituent does lead to similar patterns in the ^{19}F and ^{11}B NMR spectra, as observed for **1-4**.¹⁸ The inequivalence of the fluorine nuclei in closely related systems (e.g., **F**)⁹ has been attributed to the magnetic anisotropy associated with the current of the chelate ring π -system, with F^2 experiencing greater shielding (average ^{19}F $\delta = -139$ ppm) than F^1 (average ^{19}F $\delta = -130$ ppm). Here, the rigid, near-orthogonal arrangement of the phenanthridinyl unit relative to the azaoxaborinine chelate enables close contact between the hydrogen in the 3-position of the phenanthridinyl ring and one of the two fluorine nuclei (F^1), which can be observed by ^{19}F - ^1H NOE NMR spectroscopy (Figure 2b), suggesting that this interaction contributes to the less shielded ^{19}F resonance frequency of F^1 . This is highlighted by the strong linear correlation between the $\text{B}-\text{F}^1 \cdots \text{C}_3\text{H}^{\text{phenanthridinyl}}$ distance (obtained from the solid-state structures) and the ^{19}F resonance frequency of F^1 (Figure S1), with the shortest $\text{B}-\text{F}^1 \cdots \text{C}_3\text{H}^{\text{phenanthridinyl}}$ separation of the neutral complexes (**2**) exhibiting the greatest deshielding in the $^{19}\text{F}(\text{F}^1)$ resonance frequency.

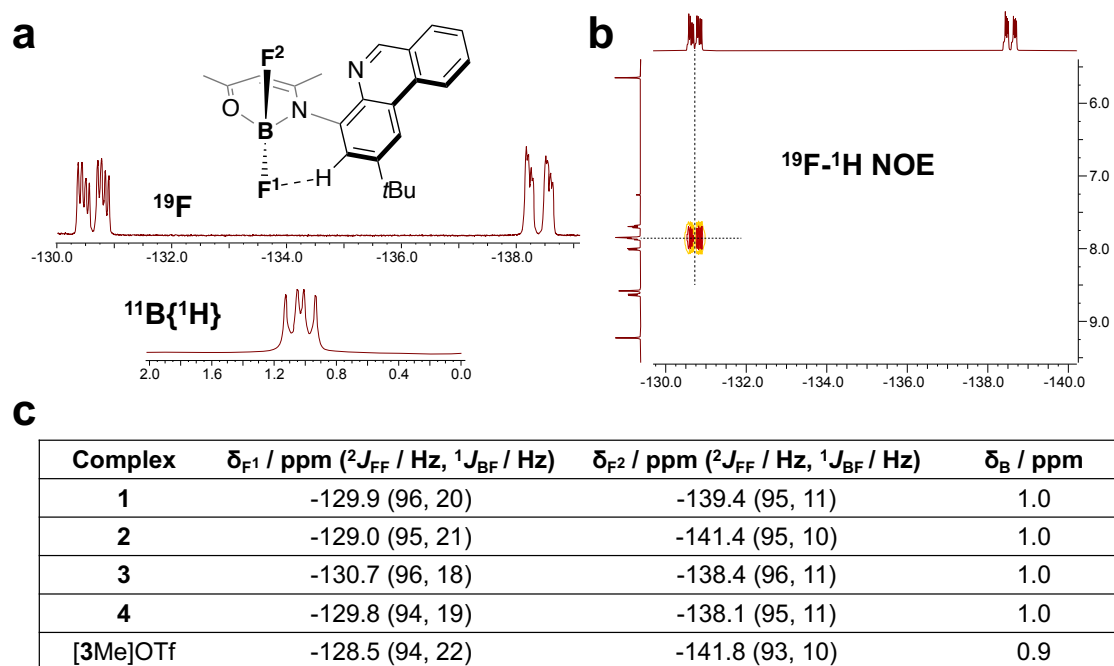


Figure 2. (a) ${}^{19}\text{F}$, ${}^{11}\text{B}$ and (b) ${}^{19}\text{F}$ - ${}^1\text{H}$ NOE NMR spectra and (c) assignments for **1-4** and [3Me]OTf.

Reacting **3** with methyl trifluoromethanesulfonate (OTf^- , triflate) resulted in the selective methylation of the phenanthridinyl nitrogen, generating the *N*-methylated phenanthridinium salt [3Me]OTf. A pronounced downfield shift in the C_6H resonance of 0.8 ppm is observed, accompanied by a downfield shift of the methine C_{13}H resonance by 0.2 ppm compared with **3**. In addition, a new methyl ${}^1\text{H}$ resonance appears at 4.63 ppm (C_{18}H), which is far more downfield than the ${}^1\text{H}$ resonances of the C_{11}H (2.35 ppm) and C_{15}H (2.03 ppm) methyl substituents of the azaoxaborinine chelate ring. The appearance of a new ${}^{19}\text{F}$ resonance with the correct integration for OTf^- further supports the structural assignment, as does the high-resolution mass spectrum.

Methylation also induces steric repulsion between the *N*-methyl substituent and the BF_2 unit, leading to a greater difference between the magnetic environments of the two F

atoms, as indicated by a downfield shift of the signal for F¹ (δ_F : -128.5 ppm, [3Me]OTf; *cf.* -130.7 ppm, **3**) and an upfield shift of that of F² (δ_F : -141.8 ppm, [3Me]OTf; -138.4 ppm, **3**). The more imposing N-Me unit increases the interaction between F¹ and the phenanthridinyl C₃H in two ways. First, the phenanthridinyl moiety tilts to move the N-Me unit away from the (N[^]O)BF₂ unit, in turn pushing the H atom in the 3-position closer as illustrated in Figure S2. Second, the boron center unit drops slightly more out of the plane formed by the ligand, evidenced by changes to the angle between the plane formed by the N-C-C-C-O ligand backbone and that formed by the N-B-O unit (20.0°, [3Me]⁺; 13.2°, **3**; ground state equilibrium geometries in CH₂Cl₂ at the SMD-CAM-B3LYP-D3(BJ)/def2-SVP level of theory). This is accompanied by a slight upfield shift of the ¹¹B resonance ($\delta(^{11}\text{B})$: 0.9 ppm, [3Me]OTf; 1.0 ppm, **3**). A further consequence is a weaker interaction between F² and the boron center in solution, as evidenced by a less well-resolved ¹J_{BF} coupling constant and a broader signal in both ¹⁹F and ¹¹B spectra compared to **3**, suggesting elongation of the B–F bond. The ²J_{FF} coupling constant is also slightly reduced in [3Me]OTf (**3**: ²J_{FF} = 96 Hz; [3Me]OTf: ²J_{FF} = 94 Hz).

Solid-State Structures. The nuclearity and binding modes of the complexes in the solid state were confirmed using single crystal X-ray diffraction (Figure 3a-d). Suitable crystals of **1**, **2**, **4** and [3Me]OTf were grown by the slow diffusion of hexanes or pentane vapors into chloroform solutions. In each structure, the boron center is monomeric and four-coordinate. Consistent with literature boron complexes supported by ketoiminate ligands,^{9,30–32} the B–N bonds (1.562 Å average) are ~0.09 Å longer than the B–O bonds (1.469 Å; Table 1). Compared with symmetric boron diketonates, diketoiminates and

diiminates,⁹ the BF₂ unit is displaced further away from the plane of the chelate ring which causes the F–B–F angle to become more acute and a downfield shift to the ¹¹B NMR resonance. The C–N and C–O bonds of the chelate ring are shorter and longer across the series, respectively, than in the solid-state structure of the proligand **L3**.²⁵ This suggests a switch from keto-enamine to enolato-imine tautomeric structure upon deprotonation and binding to boron (Figure 3e). Solid-state IR spectra support this assignment, which is also corroborated by DFT-calculated IR spectra [CAM-B3LYP-D3(BJ)/def2-SVP; gas-phase]. For example, the vibrational mode attributable to the C–O stretch shifts to lower energy in the BF₂ complexes compared with the free ligands ($\nu_{\text{C=O, stretch}} / \text{cm}^{-1}$: **L1** 1617 vs **1** 1397; **L2** 1615 vs **2** 1404; **L3** 1617 vs **3** 1403; **L4** 1634 vs **4** 1524). A similar shift to lower frequency of the C–O stretch was observed for a series of (*N*-methyl-1,3-enaminoketonato)boron difluorides.³³

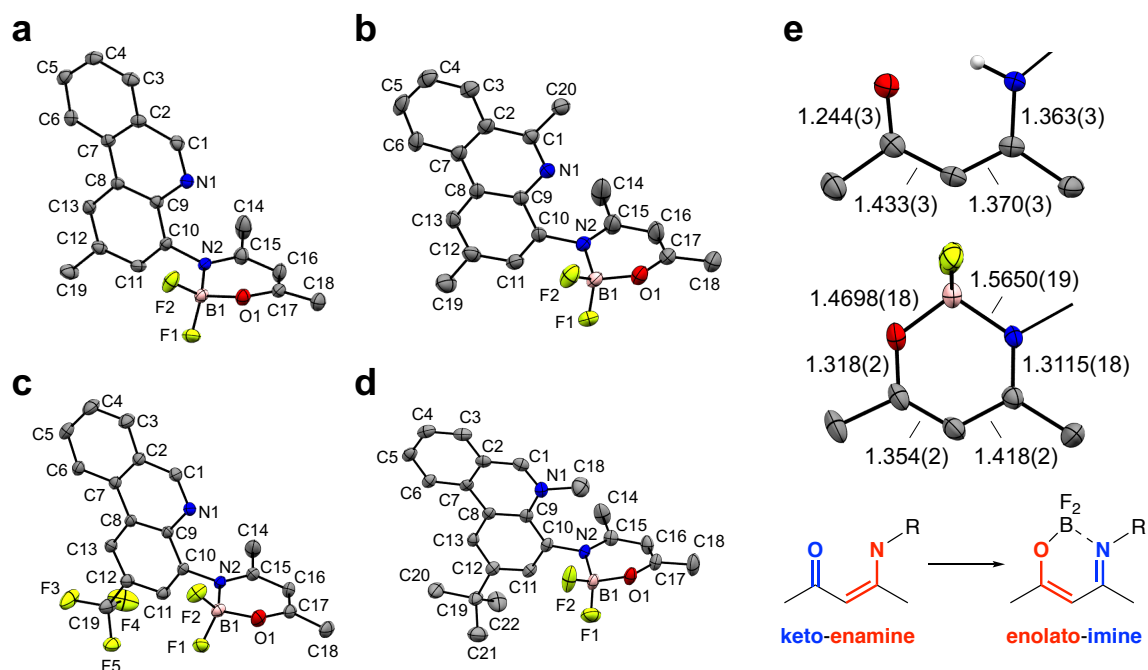


Figure 3. Solid-state X-ray structures of (a) **1**, (b) **2**, (c) **4**, and (d) [3Me]OTf, with thermal ellipsoids shown at 50% probability level. Hydrogen atoms, counterion, and co-crystallized solvents are omitted for clarity. (e) Bonding description highlighting keto-enamine tautomer in proligand **L3**²⁵ and enolato-imine tautomer in **4**.

As concluded in solution, the phenanthridinyl arms are not associated with the boron centers in the solid state. In each structure, the phenanthridinyl ring is nearly orthogonal to the plane formed by the B-N-C-C-C-O backbone of the (N⁺O)BF₂ unit (**1**, 86.4°; **2**, 81.2°; **4**, 87.4°; [3Me]⁺: 88.7°; Figure S3a). The small variation between the complexes is likely ascribable to packing effects rather than to any electronic influence of the substituents, as values for the optimized ground-state geometries of the neutral boron complexes in the gas phase are predicted to lie within an even narrower range (69-71°), while the cationic analogue displays a slight decrease relative to the solid-state structure (81.7°). The (N⁺O)BF₂ rings are not completely planar, thanks to the preference of the four-coordinate boron for a pseudo-tetrahedral geometry, and the boron nucleus lies to one side of the plane formed by the N-C-C-C-O atoms of the ligand backbone, distinguishing the two B-F bonds, consistent with the solution-phase assignment described above (Figure S3b). Analysis of extended interactions in the solid state suggests that this deviation from planarity is not only influenced by crystal packing, but also by weak intermolecular CH⁺⋯F non-covalent interactions³⁴ and intramolecular steric repulsion between the phenanthridinyl moiety and (N⁺O)BF₂ unit (Figures S4-S7). As discussed above, the BF₂ unit in each structure leans toward the C11-*H* unit and away from the C=N subunit, with B1-F1⋯C11-*H* and B1-F2⋯N1=C1 separations of 2.9 Å and 3.4 Å, respectively. The

solid-state structure of [3Me]⁺ shows that both the out-of-plane positioning of the boron relative to the chelate plane ([3Me]⁺: 27.7°; cf. **1**, 25.1°; **2**, 20.6°; **4**, 12.1°; the BF₂ “pucker” angle in Table 1) and the tilting of the phenanthridinyl plane relative to the chelate plane increase upon *N*-methylation, resulting from the mutual repulsion between the methyl and the BF₂ units, as predicted by the solution NMR data. The B1–F2 bond distance is also elongated by 0.017 Å compared with B1–F1. This is consistent with the smaller ¹J_{BF} and ²J_{FF} coupling constants measured for [3Me]⁺ compared to **3**.

Table 1. Selected bond lengths (Å), bond angles (°), and dihedral angles (°) between the boron difluoride chelate and phenanthridine planes.

| Complex | 1 | 2 | 4 | [3Me] ⁺ |
|---------------------------------------|----------|----------|------------|--------------------|
| B1–O1 | 1.467(3) | 1.471(4) | 1.4698(18) | 1.472(5) |
| B1–N2 | 1.563(4) | 1.558(4) | 1.5650(19) | 1.558(5) |
| B1–F1 | 1.374(3) | 1.379(3) | 1.3751(19) | 1.358(5) |
| B1–F2 | 1.376(3) | 1.380(3) | 1.3841(19) | 1.375(5) |
| O1–B1–N2 | 108.6(2) | 109.4(2) | 109.48(12) | 108.5(3) |
| F1–B1–F2 | 110.7(2) | 110.1(2) | 109.86(13) | 111.4(3) |
| O1–B1–F1 | 109.5(2) | 108.3(2) | 109.84(12) | 109.3(3) |
| O1–B1–F2 | 108.9(2) | 109.8(2) | 108.99(12) | 109.3(3) |
| N2–B1–F1 | 109.3(2) | 110.3(2) | 109.78(11) | 109.5(3) |
| N2–B1–F2 | 109.8(2) | 109.0(2) | 108.87(12) | 108.7(3) |
| Interplanar angle ^a | 86.4 | 81.2 | 87.4 | 88.7 |
| BF ₂ “pucker” ^b | 25.1 | 20.6 | 12.1 | 27.7 |

^a Angle between calculated planes of phenanthridinyl and the (N[^]O)B chelate ring (see Figure S3a).

^b Angle between N2-C15-C16-C17-O1 and N2-B1-O1 planes (see Figure S3b).

Absorption and Emission Spectroscopy

Compounds **1-3** are pale brown or orange (**4**) as powders and light yellow in solution. Solution UV-vis absorption spectra accordingly lack significant absorptive cross-section in the visible region of the spectrum but contain three notable features in the UV: two

intense absorptions at ~ 225 and 300 nm, and a weak but sharp peak on the low-energy edge of these bands at ~ 350 nm (Figure 4). Such features have been observed in Pt(II) complexes with phenanthridinyl-based ligands related to those here.^{35,36} Indeed, a series of relatively weak but well-resolved bands around 350 nm is typical of the 1L_b π - π^* transitions of azaphenanthrenes including phenanthridine.³⁷⁻³⁹ The lowest-energy singlet excited state of the heterocycles remains similar to that of phenanthrene itself, despite the introduction of the heteroatom, and its energy is largely insensitive to the local environment. In the present instance, no significant solvatochromism was observed in the spectrum, consistent with this assignment. *N*-Methylation to generate [3Me]OTf results in a red-shift and the absorption then tails to ~ 400 nm, consistent with the effect of protonation or *N*-methylation of phenanthridine itself.^{40,41}

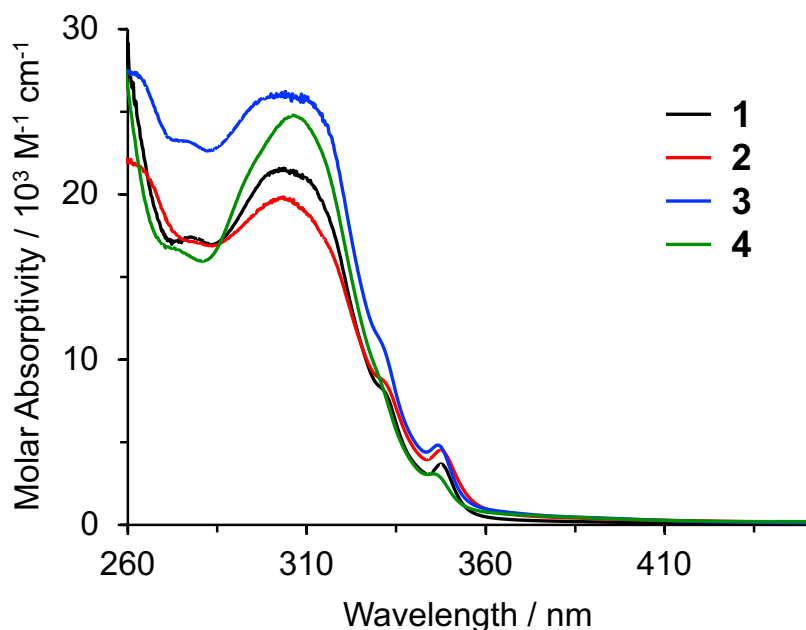


Figure 4. UV-Vis absorption spectra of **1-4** in CH_2Cl_2 at 295 K.

For complexes **1–4** in deoxygenated dichloromethane, excitation into the lowest energy manifold (~350 nm) produces only very weak, broad emission in the 360–600 nm region. The most convincing data were obtained for compound **3** (Figure 5a), with an emission maximum around 370 nm, resembling fluorescence from phenanthridine itself but lacking the expected vibrational structure and with a much lower quantum yield (1% versus 19% for phenanthridine⁴⁰). The excitation spectrum of **3** does show reasonable agreement with the absorption spectrum, but for **1**, **2**, and **4**, the excitation spectra show bands that extend to longer wavelength than the absorption spectrum. Strikingly, the *N*-methylated compound [3Me]OTf is much more brightly emissive, showing a broad, unstructured emission band centered at 508 nm in deoxygenated CH₂Cl₂ with a quantum yield and emission decay time of 9 ± 2 % and 2.7 ± 0.5 ns (Figure 5b), respectively. The absorption and excitation spectra now show a convincing match. There is no significant change in the quantum yield or lifetime in air-equilibrated solution compared to the deoxygenated conditions. The short lifetime and lack of sensitivity to dissolved oxygen point to the emission being spin-allowed fluorescence from a singlet excited state. The emission is, however, significantly red-shifted by about 100 nm compared to *N*-methylated phenanthridines,⁴¹ and thus is unlikely to emanate from a simple phenanthridine-localised excited state. The emission band shows only a small degree of positive solvatochromism, being slightly blue-shifted in THF ($\lambda_{\text{max}} = 504$ nm) and slightly red-shifted in MeCN ($\lambda_{\text{max}} = 514$ nm; Figure S8). The quantum yield is reduced relative to that in CH₂Cl₂ in both cases (1.1 and 1.9 %, respectively).

At 77 K, all five compounds display two sets of vibrational bands, one in the region 360–420 nm and the other roughly between 460–600 nm. These two sets are consistent

with the fluorescence and phosphorescence bands, respectively, displayed by phenanthridine at low temperature.⁴² This assignment is supported by very different emission decay times (τ) of the two sets of bands (9.6 ns and 750 ms, in the case of [3Me]OTf) corresponding to spin-allowed and formally spin-forbidden transitions respectively. The lifetimes of the phosphorescence bands of **1**, **3** and **4** were similar ($\tau = 870, 880, 820$ ms; the estimated uncertainty is $\pm 10\%$), whilst that of **2** was a little longer at 1300 ms. Interestingly, the ratio of the integrated intensities of the fluorescence to phosphorescence bands is much higher for the methylated compound (ratios are approximately 3.5:1 for [3Me]OTf and 1:4 for **3**), which might indicate that the rate of intersystem crossing (ISC) has been retarded upon methylation. ISC competes with fluorescence as a deactivation pathway for the singlet state, and thus a reduction in the rate of ISC may lead to an increase in fluorescence. Meanwhile, a reduction in ISC also limits the yield of triplet state upon light absorption, lowering the contribution from phosphorescence. Such an effect might also account, at least in part, for the more intense fluorescence exhibited by [3Me]OTf at room temperature. However, the earlier conclusion that the room temperature fluorescence is not solely phenanthridine-based is reinforced by the large bathochromic shift of the fluorescence by around 5000 cm^{-1} on going from 77 K to room temperature, much larger than typical rigidochromic effects for aromatics.

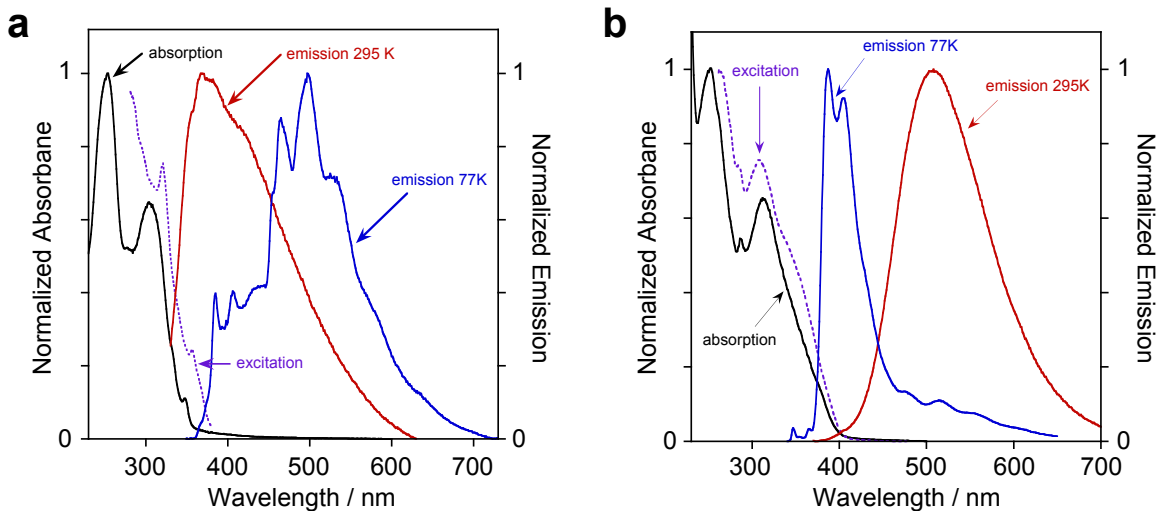


Figure 5. Absorption and emission spectra of (a) **3** and (b) **[3Me]OTf**.

Electronic Structure Calculations. Density functional theory (DFT) calculations were carried out on **1-4** and **[3Me]⁺** to interpret the characterization data discussed above. Gas-phase optimizations of all compounds were first performed using the CAM-B3LYP functional which has been shown to model donor-acceptor complexes containing BF₂ in good agreement with experiment.⁴³ The structures of **3** and **[3Me]⁺** were also optimized using the solvation model based on density approach⁴⁴ (SMD; CH₂Cl₂). The structural metrics so-obtained are in good agreement with the solid-state structures (Table S1), with the notable exception of the angle between the (N[^]O)B chelate plane and that of the phenanthridinyl subunit, which is larger in the solid state likely due to packing effects. Better agreement is obtained for **[3Me]⁺** (gas phase DFT, 81.7°; SMD, 81.2°; X-ray, 88.7°).

Energies and isosurfaces of selected ground-state molecular orbitals (MOs) of **3** and **[3Me]⁺** are presented in Figure 6 (MO energy level diagrams of **1-4** in the gas phase are provided as Figure S9). For **1-4**, the three lowest energy vacant orbitals have both phenanthridinyl (LUMO+2/LUMO+1/LUMO: **1**, 48/77/78; **2**, 50/79/68; **3**, 51/74/77; **4**,

37/77/88%) and oxazaborinine (LUMO+2/LUMO+1/LUMO: **1**, 51/22/21; **2**, 48/17/28; **3**, 49/24/21; **4**, 63/22/10%) character (see Tables S2-S8). The highly electron-withdrawing CF₃ substituent in **4** stabilizes the *N*-heterocyclic fragment, and the LUMO of **4** has the lowest oxazaborinine and highest phenanthridinyl character of the series. The phenanthridinyl substituents do not appear to impact the calculated HOMO-LUMO gaps, mirroring the similarity in $\lambda_{\text{abs,max}}$ for **1-4**, while the bathochromic shift to the lowest energy manifold of [3Me]⁺ compared to **3** is reproduced by computation. As with coordination complexes of Lewis acidic metal ions supported by phenanthridine-based ligand scaffolds,⁴⁵⁻⁴⁷ the LUMO has particularly localized orbital density at the C=N subunit of the phenanthridinyl, consistent with ‘imine-bridged biphenyl’ character to the tricyclic moiety. This is accentuated upon methylation of the phenanthridinyl nitrogen, such that the LUMO of **3** has 70% phenanthridine character, 21% of which is localized at the C=N subunit, while the comparable numbers for [3Me]⁺ are 94% and 38%. The HOMO and HOMO-2 also show mixed phenanthridinyl (HOMO/HOMO-2: **1**, 63/41; **2**, 69/39; **3**, 62/40; **4**, 35/62) and oxazaborinine character (HOMO/HOMO-2: **1**, 34/57; **2**, 26/60; **3**, 36/59; **4**, 64/37). The HOMO-1, in comparison, has dominant phenanthridinyl character and only a small but non-negligible oxazaborinine contribution in **1-3** which drops to zero in **4**. Solvation has a minor impact on the energies of the MOs and a similar HOMO-LUMO gap is predicted for **3** in vacuum (6.52 eV) vs. CH₂Cl₂ (6.66 eV). The characters of the HOMO and HOMO-2, however, are quite different. The oxazaborinine contribution to the HOMO of **3** decreases from 36% in the gas phase to 6% in CH₂Cl₂, while a similar decrease in the phenanthridinyl contribution is observed for the HOMO-2 (vacuum: 40%; CH₂Cl₂: 28%).

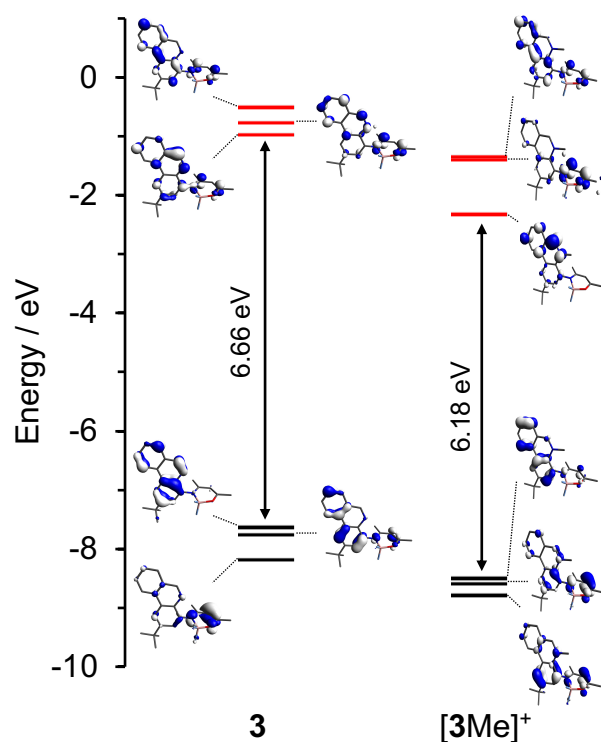


Figure 6. Selected molecular orbitals (SMD-RIJCOSX-rM06-2X/def2-TZVP(-f)+def2/J//SMD-rCAM-B3LYP-D3(BJ)/def2-SVP; solvent = CH₂Cl₂) of **3** and [3Me]⁺ (isovalue = 0.04) and their relative energies.

Comparing **3** with its *N*-methylated congener [3Me]⁺, the HOMO and LUMOs of the two complexes have somewhat inverted character. In **3**, the HOMO has dominant (89%) phenanthridinyl character, while the LUMO has mixed (70:29%) phenanthridinyl/(N⁺O)B character. In [3Me]⁺, the LUMO has dominant (94%) phenanthridinyl character, while the HOMO has more mixed 83:15 phenanthridinyl/(N⁺O)B chelate character. Overall, methylation enhances the phenanthridinium character to both frontier orbitals, which leads to the lowest energy

transitions of this compound being of π - π^* local excitation (LE) character, consistent with the lack of pronounced solvatochromism.

TDDFT simulations were then conducted for **3** and $[\mathbf{3Me}]^+$ both in vacuum and CH_2Cl_2 (Figures S10-S13). These calculations reveal that the major transitions responsible for the UV-Vis absorption spectrum of **3** present significant mixed character due to configuration interactions and cannot be fully attributed to HOMO-LUMO transitions. Electron-hole difference density maps (Figures S14-S15) of the three dominant ($f_{\text{osc}} > 0.01$) transitions of **3** all indicate oxazaborinine \rightarrow phenanthridine charge-transfer character. Accordingly, we calculate a significant change in the dipole moment relative to the ground-state for each of these excited-states ($\Delta\mu$ (CH_2Cl_2): S_1 9.5 D, S_2 10.2 D, S_4 9.8 D). In comparison, the lowest energy transitions calculated for $[\mathbf{3Me}]^+$ have much more significant locally excited π - π^* character originating from the redistribution of electron density within the phenanthridinyl moiety. The calculated change in dipole moment is accordingly smaller ($\Delta\mu$ (CH_2Cl_2): S_1 5.7 D, S_2 7.5 D).

While the excitations associated with the lowest energy absorption of **3** and $[\mathbf{3Me}]^+$ are therefore clearly different, they are not so distinct as to explain the ‘switching-on’ of emission in the methylated congener. We therefore proceeded to examine the potential energy surfaces (PES) of the ground-state, two lowest-lying excited singlet states (S_1 and S_2), and lowest-lying excited triplet state (T_1) of **3** by scanning about the phenanthridinyl-oxazaborinine dihedral along the C-N bond adjoining these units and allowing for molecular relaxation after each rotation (Figure S16, gas-phase; Figure S17, CH_2Cl_2). Gas phase and solution scans gave similar results, so we limit our discussion to the solution PES. Two minima are observed in the ground state with an associated transition energy of

1.4-1.7 eV. The rotation about the C-N bond connecting the phenanthridinyl and oxazaborinine units involves a transition state where the phenanthridinyl and (N[^]O)B ring planes approach co-planarity, causing the geometry at the (N[^]O) nitrogen to become less planar in order to minimize unfavorable steric repulsion between the two fragments. The steep descent from the maxima indicates a discontinuity which could be from BF₂ dissociation from the ligand – this may provide a pathway for non-radiative decay.

The excited singlet (S₁, S₂) and triplet (T₁) states show multiple shallow minima which more or less coincide with the maxima of the ground state PES of **3**. These minima are defined by reduced planarity at the (N[^]O) nitrogen atom, such that the phenanthridine and (N[^]O)BF₂ units hinge about this atom. Such ‘butterfly modes’ have been invoked in formazanate ligand BF₂ complexes to explain non-emissive excited states.⁴⁸ The PES of the excited singlet and triplet states exhibit several energetically close structures which could facilitate rapid intersystem crossing (ISC) to the low-lying excited triplet state through vibronic coupling and may explain the observed ratio of the integrated intensities of the fluorescence to phosphorescence bands in **3** (1:4). Methylation rigidifies [**3Me**]⁺ compared to **3** and likely increases the barrier associated with the rotation about the phenanthridine-oxazaborinine connecting C-N bond. If ISC from S₁ to T₁ requires a change in geometry as described above, this rigidification may serve to inhibit ISC. Indeed, at 77 K, the fluorescence:phosphorescence ratio observed for [**3Me**]⁺ has increased to 3.5:1. The similarity of the orbital characters of the S₁ and S₂ states (¹π-π*) and the T₁ state (³π-π*) could similarly disfavor ISC. In comparison, in **3**, we find more pronounced difference in the characters of the low-lying excited singlet states compared with the triplet state. While the excited singlet states of **3** exhibit some CT character, the triplet state is predominantly

phenanthridinyl π - π^* character (Figure S18). As per El-Sayed's rule,⁴⁹ differences in the orbital characters between the low-lying excited singlet and triplet states should enhance spin-orbit coupling between these states and facilitate efficient ISC. This also could contribute to the increased quantum yield in [3Me]OTf compared to **3** in fluid solution.

Furthermore, the anomalous excitation spectra of **1-4** with respect to their UV-Vis absorption spectra can be explained in light of the shallow PES of the excited states. Closely related oxazaborinines exhibit extremely weak emission in solution but become emissive in the solid-state.^{9,18} Restriction of such motions as described above in the solid-state could explain the increased emission. Complexes **1-4** do not emit in the solid-state, likely due to aggregation-induced quenching, but they are emissive in frozen glass at 77 K as discussed earlier. The spin density of the T₁ states of **3** and [3Me]⁺ (Figures S18-S19) indicates phenanthridinyl π - π^* character to both, in line with our earlier interpretation of phenanthridine-like fluorescence and phosphorescence.

Conclusions

In this work, we present a series of four intramolecular, donor-stabilized BF₂ complexes supported by phenanthridinyl-decorated β-ketoiminate chelating ligand scaffolds. The complexes are characterized in solution using multinuclear NMR and IR spectroscopy, and in the solid-state by X-ray diffraction. In solution, the relative orientation of the pendent phenanthridinyl arm is fixed despite not coordinating to the boron center, and a well-resolved through-space interaction between a phenanthridinyl C-H and a single fluorine atom can be observed by ¹⁹F-¹H NOE NMR spectroscopy. Despite this fixed orientation, the neutral compounds are only weakly emissive in fluid solution, ascribed to non-radiative decay pathways enabled by rotation of the *N*-heterocyclic unit. Methylation of the phenanthridinyl nitrogen restricts this rotation and switches on comparably strong emission in solution. At low temperature, emission from **3** and its methylated congener [3Me]OTf is similar but with key differences in the relative amounts of fluorescence and phosphorescence, supporting the proposed role for increased molecular rigidity and the influence of methylation on the rate of ISC. The calculated potential energy surfaces of the neutral complexes are accordingly quite shallow. Density functional theory (DFT) and time-dependent DFT (TDDFT) modelling indicates that the character of the lowest energy excitations changes upon methylation, accentuating phenanthridine character to the frontier orbitals and inhibiting intersystem crossing which helps boost emission from spin-allowed singlet excited states.

Experimental Section

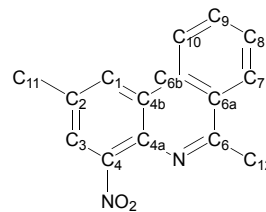
General Considerations

Air-sensitive manipulations were carried out in an N₂-filled glove box or using standard Schlenk techniques under Ar. 6-Iodo-4-methyl-2-nitroaniline,²⁶ 4-amino-(2-methyl)phenanthridine,²⁶ **L3**²⁵ and **L4**²⁵ were synthesized according to literature procedures. 2-Acetylphenylboronic acid (Combi-Blocks), acetylacetone (Sigma-Aldrich), *p*-toluenesulfonic acid monohydrate (Sigma-Aldrich), boron trifluoride diethyl etherate (Alfa Aesar) and other common reagents were purchased from commercial suppliers and used without further purification. Organic solvents were dried and distilled using appropriate drying agents. 1- and 2D NMR spectra were recorded on a Bruker Avance 300 MHz spectrometer or a Bruker Avance 500 MHz spectrometer. Structural assignments were made with additional information from gCOSY, gHSQC, and gHMBC experiments. ¹H and ¹³C{¹H} NMR spectra were referenced to residual solvent peaks. High resolution mass spectra were recorded using a Bruker microOTOF-QIII. Attenuated total reflectance infrared spectroscopy (ATR-IR) was collected using a Bruker Invenio R FTIR or a Perkin Elmer Spectrum Two FTIR spectrometer. X-ray crystal structure data was using collected on a Bruker D8 QUEST ECO diffractometer from multi-faceted crystals of suitable size and quality selected from a representative sample of crystals of the same habit using an optical microscope. In each case, crystals were mounted on MiTiGen loops and data collection carried out in a cold stream of nitrogen (150 K; Mo K α radiation). All diffractometer manipulations were carried out using Bruker APEX3 software.⁵⁰ Structure solution and refinement was carried out using XS, XT and XL software, embedded within

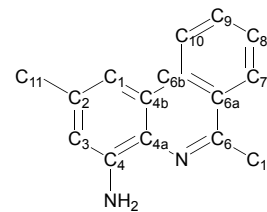
OLEX2.⁵¹ For each structure, the absence of additional symmetry was confirmed using ADDSYM incorporated in the PLATON program.⁵²

Synthesis

2,6-Dimethyl-4-nitrophenanthridine: A Teflon-stoppered flask was charged with Pd(PPh₃)₄ (1.05 g, 0.913 mmol), 2-iodo-4-methyl-6-nitroaniline (5.06 g, 18.2 mmol), 2-acetylphenylboronic acid (3.59 g, 21.9 mmol), Na₂CO₃ (6.76 g, 63.8 mmol), 1,2-dimethoxyethane (80 mL), and water (70 mL). The biphasic mixture was refluxed for 16 h in an oil bath set to 130 °C, after which the mixture was cooled and the organic solvent evaporated *in vacuo*. The crude product was extracted from the isolated aqueous fraction with CH₂Cl₂ (2 × 75 mL) and isolated as a brown solid after evaporation of CH₂Cl₂. A spectroscopically pure, brown solid was isolated after stirring overnight in methanol at room temperature. A spectroscopically pure, brown solid was isolated following stirring in methanol at room temperature. Isolated yield = 3.05 g (75%). ¹H NMR (CDCl₃, 500 MHz, 25 °C): δ 8.48 (d, *J*_{HH} = 8.3 Hz, 1H; C₁₀H), 8.35 (s, 1H; C₁H), 8.15 (d, *J*_{HH} = 8.0; C₇H), 7.82 (ddd, *J*_{HH} = 8.6, 7.6, 1.3 Hz, 1H; C₉H), 7.70 (ddd, *J*_{HH} = 8.7, 7.7, 1.3 Hz, 1H; C₈H), 7.67 (s, 1H; C₃H), 2.95 (s, 1H; C₁₂H), 2.60 (s, 1H; C₁₁H). ¹³C {¹H} NMR (CDCl₃, 125 MHz, 25 °C): δ 160.9 (C₆), 148.8 (C₄), 135.5 (C_{4a}), 133.4 (C_{6a}), 131.1 (C₉ and C_{6b}), 128.5 (C₈), 126.8 (C₇), 126.2 (C_{4b}), 125.1 (C₂), 125.0 (C₁), 123.1 (C₃), 122.5 (C₁₀), 23.7 (C₁₂), 21.7 (C₁₁). HR-MS (APCI-TOF) *m/z*: [M + H]⁺ calcd for [C₁₅H₁₂N₂O₂]⁺ 253.0972; Found 253.0977.

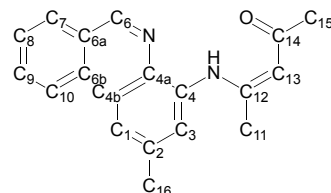


4-Amino-2,6-dimethylphenanthridine: 2,6-dimethyl-4-nitrophenanthridine (3.65 g, 14.5 mmol), hydrazine hydrate (18.5 mL), formic acid (2.5 mL), and zinc (1.89 g, 28.9 mmol) were



refluxed for 16 h in MeOH (90 mL). After cooling to room temperature, the mixture was vacuum-filtered to give a yellow solution, which was concentrated *in vacuo*. The product was isolated after addition of water into the concentrated solution. Brown solid. Isolated yield = 3.01 g (94%). The isolated product was used without further purification. ^1H NMR (CDCl_3 , 500 MHz, 25 °C): δ 8.55 (d, $J_{\text{HH}} = 8.5$ Hz, 1H; C_{10}H), 8.16 (d, $J_{\text{HH}} = 8.5$ Hz, 1H; C_7H), 7.77 (ddd, $J_{\text{HH}} = 8.7$ Hz, 7.7 Hz, 1.6 Hz, 1H; C_9H), 7.61-7.68 (overlapping s and m, 2H; C_1H and C_8H), 6.83 (s, 1H; C_3H), 5.07 (br s, 2H; NH) 3.00 (s, 1H; C_{12}H), 2.50 (s, 1H; C_{11}H). $^{13}\text{C}\{^1\text{H}\}$ NMR (CDCl_3 , 125 MHz, 25 °C): δ 154.7 (C_6), 143.9 ($\text{C}_{6\text{b}}$), 136.9 (C_2), 132.8 ($\text{C}_{6\text{a}}$), 130.9 (C_4), 130.1 (C_9), 127.0 (C_8), 126.5 (C_7), 126.3 ($\text{C}_{6\text{a}}$), 124.2 ($\text{C}_{4\text{a}}$), 122.9 (C_{10}), 113.0 (C_3), 110.8 (C_1), 23.3 (C_{12}), 22.4 (C_{11}). HR-MS (APCI-TOF) m/z : $[\text{M} + \text{H}]^+$ calcd for $[\text{C}_{15}\text{H}_{14}\text{N}_2]^+$ 223.1230; Found 223.1237.

4-(4-Enamino-2-methylphenanthridinyl)-3-penten-2-one

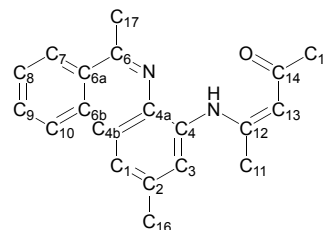


(L1): A Teflon-stoppered flask was charged with (4-amino-2-methyl)phenanthridine (1.00 g, 4.80 mmol), acetylacetone (1.5 mL, 15 mmol), 4-toluenesulfonic acid monohydrate (0.0459 g, 0.241 mmol) and 4 Å molecular sieves (7 g). The mixture was sealed and stirred at reflux for 48 h in an oil bath set to 130 °C. The reaction mixture was cooled and filtered, and the filtrate concentrated to give a dark brown viscous oil. The product was precipitated as a brown solid by addition of diisopropylether (20 mL) and isolated by filtration, giving a spectroscopically pure product which could be used without further purification. Isolated yield = 1.00 g (72 %). ^1H NMR (CDCl_3 , 300 MHz, 25 °C): δ 13.53 (b s, 1H; NH), 9.29 (s, 1H; C_6H), 8.55 (d, $^3J_{\text{HH}} = 8.2$ Hz, 1H; C_{10}H), 8.06 (s, 1H; C_1H), 8.04 (dd, $^3J_{\text{HH}} = 8.1$ Hz, $^4J_{\text{HH}} = 0.6$ Hz, 1H; C_7H), 7.69 (m, 1H; C_8H), 7.83 (m, 1H; C_9H), 7.34 (d, $^4J_{\text{HH}} = 1.1$ Hz, 1H; C_3H), 5.33 (s, 1H; C_{13}H),

2.59 (s, 3H; C₁₆H), 2.26 (s, 3H; C₁₁H), 1.18 ppm (s, 9H; C₁₅H). ¹³C{¹H} NMR (CDCl₃, 75 MHz, 25 °C): δ 196.4 (C₁₄), 158.2 (C₁₂), 151.9 (C₆), 137.2 (C₄), 136.7 (C_{4a}), 135.7 (C₂), 132.2 (C_{4b}), 130.9 (C₉), 128.9 (C₇), 127.7 (C₈), 126.8 (C_{6a}), 124.8 (C_{6b}), 122.2 (C₁₀), 121.6 (C₃), 117.5 (C₁), 100.1 (C₁₃), 29.6 (C₁₅), 22.6 (C₁₆), 21.4 ppm (C₁₁). IR (ATR): ν_{max} 3100-2800 (C-H stretch, broad, w), 1617 (C=O stretch, sharp, m), 1569 cm⁻¹ (N-H bend, sharp, s). HRMS (APCI-TOF) m/z: [M + H]⁺ calcd for [C₁₉H₁₈N₂O]⁺ 291.1942; Found 291.1493.

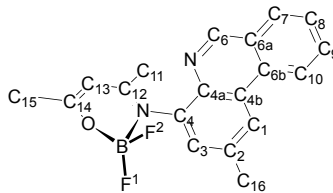
4-(2,6-Dimethyl-4-enaminophenanthridinyl)-3-penten-2-one

(L2): The above procedure was followed using 2,6-dimethyl-4-aminophenanthridine (1.00 g, 4.50 mmol), acetylacetone (1.4 mL, 14 mmol), 4-toluenesulfonic acid monohydrate (0.0470 g,



0.247 mmol), and 4 Å molecular sieves (7 g) in toluene (10 mL). Brown solid. Isolated yield = 0.929 g (68 %). ¹H NMR (CDCl₃, 300 MHz, 25 °C): δ 13.59 (b s, 1H; NH), 8.50 (d, ³J_{HH} = 8.2Hz, 1H; C₁₀H), 8.15 (dd, ³J_{HH} = 8.3Hz, ⁴J_{HH} = 0.8 Hz, 1H; C₇H), 7.92 (s, 1H; C₁H), 7.75 (m, 1H; C₉H), 7.63 (m, 1H; C₈H), 7.329 (d, ⁴J_{HH} = 1.1Hz, 1H; C₃H), 5.33 (s, 1H; C₁₃H), 3.08 (s, 3H; C₁₇H), 2.52 (s, 3H; C₁₆H), 2.29 (s, 3H; C₁₁H), 2.17 ppm (s, 3H; C₁₅H). ¹³C{¹H} NMR (CDCl₃, 75 MHz, 25 °C): 196.0 (C₁₄), 157.4 (C₁₂), 157.0 (C₆), 136.7 (C₂), 135.6 (C_{4b}), 133.6 (C₄), 132.1 (C_{6a}), 130.3 (C₈), 127.4 (C₉), 126.6 (C₇), 126.2 (C_{6b}), 124.2 (C_{4a}), 122.6 (C₁₀), 119.9 (C₃), 116.6 (C₁), 100.4 (C₁₃), 29.7 (C₁₅), 23.9 (C₁₇), 22.6 (C₁₆), 21.8 (C₁₁). IR (ATR): ν_{max} 3100-2800 (C-H stretch, broad, w), 1615 (C=O stretch, narrow, m), 1569 cm⁻¹ (N-H bend, narrow, s). HRMS (APCI-TOF) m/z: [M + H]⁺ calcd for [C₂₀H₂₀N₂O]⁺ 305.1648; Found 305.1644.

Complex 1: In a Teflon-stoppered flask, triethylamine (148 μL , 1.07 mmol) was added to a stirring solution of **L1** (0.100 g, 344 μmol) and boron trifluoride diethyl etherate (217 μL ,

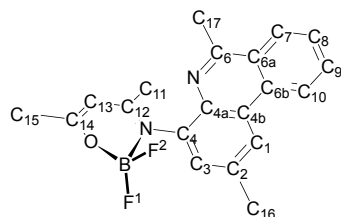


1.76 mmol) in toluene (11 mL). The mixture was heated to reflux in an oil bath set to 110°C for 16 h. A precipitate was observed to gradually form over this time. The resultant suspension was then cooled to room temperature. Addition of CH_2Cl_2 (approximately 25 mL) re-dissolved the precipitate, and the mixture was then washed with deionized water (2 x 25 mL) and 2 M HCl (2 x 25 mL). The organic layer was separated, filtered over Celite, and dried *in vacuo*. The resulting solid was re-dissolved in minimal CH_2Cl_2 and precipitated by addition of MeOH, followed by ice-cold water. The precipitate was filtered over Celite, then isolated using CH_2Cl_2 . The solution was dried over Na_2SO_4 and dried *in vacuo* to isolate a light brown solid. Isolated yield = 84 g (72 %). ^1H NMR (CDCl_3 , 300 MHz, 25 °C): δ 9.22 (s, 1H; C_6H), 8.59 (d, $^3J_{\text{HH}} = 8.2$ Hz, 1H; C_{10}H), 8.39 (s, 1H; C_1H), 8.02 (d, $^3J_{\text{HH}} = 7.9$ Hz, 1H; C_7H), 7.86 (m, 1 H; C_9H), 7.71 (m, 1H; C_8H), 7.64 (s, 1 H; C_3H), 5.65 (s, 1 H; C_{13}H), 2.65 (s, 3 H; C_{15}H), 2.25 (s, 3 H; C_{15}H), 1.87 ppm (s, 3 H; C_{11}H). ^{13}C { ^1H } NMR (CDCl_3 , 75 MHz, 25 °C): δ 176.9 (C_{14}), 173.1 (C_{12}), 153.4 (C_6), 137.9 (C_4), 137.5 (C_{4a}), 137.2 (C_2), 132.2 (C_{4b}), 131.3 (C_9), 128.9 (C_7), 128.0 (C_8), 127.9 (C_3), 126.6 (C_{6a}), 125.2 (C_{6b}), 122.4 (C_1), 122.2 (C_{10}), 99.0 (C_{13}), 23.2 (C_{15}), 22.1 (C_{15}), 21.8 ppm (C_{11}). ^{19}F NMR (CDCl_3 , 282 MHz, 25 °C): δ -129.9 (dq, $^2J_{\text{FF}} = 96$, $^1J_{\text{FB}} = 20$ Hz, 1F; BF^1), -139.4 ppm (dq, $^2J_{\text{FF}} = 95$, $^1J_{\text{FB}} = 11$ Hz, 1F; BF^2). ^{11}B NMR (CDCl_3 , 160 MHz, 25 °C): δ 1.0 ppm (dd, $^1J_{\text{BF}} = 11$ Hz, 20 Hz). IR (ATR): ν 3100-2800 (C-H stretch, broad, w), 1614 ($\text{C}_{13}=\text{N}$ stretch, narrow, m), 1534 ($\text{C}_{14}=\text{C}_{15}$ stretch, narrow, m), 1397 ($\text{C}_{15}-\text{O}$ stretch, narrow, m), 1325 ($\text{C}_{12}-\text{H}$ and $\text{C}_{16}-\text{H}$ bend, narrow, m), 1260 cm^{-1} (B-F stretch, C_6-H and C_3-H bend,

narrow, m). HR-MS (APCI-TOF) m/z : $[M + Na]^+$ calcd for $[C_{19}H_{17}N_2OBF_2Na]^+$ 361.1298; Found 361.1311.

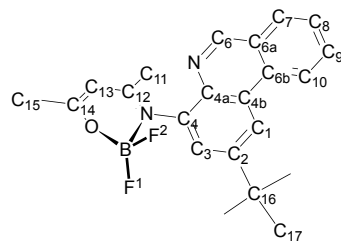
Complex 2: Following the procedure described above, triethylamine (142 μ L, 1.02 mmol) was added to a stirring solution of **L2** (0.100 g, 329 mmol) and boron trifluoride diethyl etherate (207 μ L, 1.68 mmol) in toluene (10 mL) and heated to

reflux in an oil bath set to 110°C for 16 h. Brown solid. Isolated yield = 44 mg (38 %). 1H NMR ($CDCl_3$, 300 MHz, 25 °C): δ



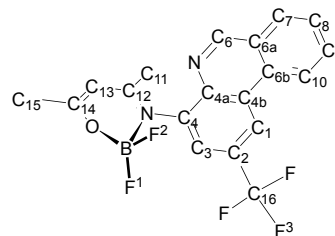
8.61 (d, $J_{HH} = 8.2$ Hz, 1H; $C_{10}H$), 8.33 (s, 1 H; C_1H), 8.18 (d, $^3J_{HH} = 8.1$ Hz, 1H; C_7H), 7.83 (m, 1 H; C_9H), 7.69 (m, 1 H; C_8H), 7.62 (s, 1 H; C_3H), 5.63 (s, 1 H; $C_{13}H$), 2.93 (s, 3 H; $C_{17}H$), 2.63 (s, 3 H; $C_{16}H$), 2.26 (s, 3 H; $C_{15}H$), 1.88 ppm (s, 3 H; $C_{11}H$). $^{13}C\{^1H\}$ NMR ($CDCl_3$, 75 MHz, 25 °C): δ 176.2 (C_{14}), 173.1 (C_{12}), 158.5 (C_6), 137.0 (C_4 , C_{4a}), 136.1 (C_2), 132.2 (C_{4b}), 130.5 (C_9), 127.7 (C_8), 127.5 (C_3), 126.6 (C_7), 126.1 (C_{6a}), 124.7 (C_{6b}), 122.6 (C_{10}), 122.1 (C_1), 98.9 (C_{13}), 23.9 (C_{17}), 23.1 (C_{15}), 22.1 (C_{16}), 22.0 ppm (C_{11}). ^{19}F NMR ($CDCl_3$, 282 MHz, 25 °C): δ -129.0 (dq, $^2J_{FF} = 95$, $^1J_{FB} = 21$ Hz, 1F; BF^1), -141.4 ppm (dq, $^2J_{FF} = 95$, $J_{FB} = 10$ Hz, 1F; BF^2). ^{11}B NMR ($CDCl_3$, 160 MHz, 25 °C): δ 1.0 ppm (dd, $^1J_{BF} = 10$, 21 Hz). IR (ATR): ν 3100-2800 (C-H stretch, b, w), 1620 ($C_{14}=N$ stretch, n, m), 1540 ($C_{15}=C_{16}$ stretch, n, m), 1404 ($C_{16}-O$ stretch, n, m), 1326 ($C_{13}-H$ and $C_{17}-H$ bend, n, m), 1261 cm^{-1} (B-F stretch, n, m). HRMS (APCI-TOF) m/z : $[M + H]^+$ calcd for $[C_{20}H_{20}N_2OBF_2]^+$ 353.1635; Found 353.1652.

Complex 3: Triethylamine (130 μ L, 0.932 mmol) was added to a stirring solution of **L3** (0.100 g, 301 mmol) and boron trifluoride diethyl etherate (189 μ L, 1.53 mmol) in toluene (9 mL) and heated to reflux in an oil bath set to 110°C for 16 h.



A spectroscopically pure brown solid was isolated. Isolated yield = 88 mg (76 %). ^1H NMR (CDCl_3 , 300 MHz, 25 °C): δ 9.23 (s, 1H; C_6H), 8.64 (d, $^3J_{\text{HH}} = 8.3$ Hz, 1H; C_{10}H), 8.58 (s, 1 H; C_1H), 8.01 (d, $^3J_{\text{HH}} = 7.9$ Hz, 1 H; C_7H), 7.87 (overlapped m, 2 H; C_3H and C_9H), 7.70 (m, 1 H; C_8H), 5.65 (s, 1 H; C_{13}H), 2.25 (s, 3 H; C_{11}H), 1.87 (s, 3 H; C_{15}H), 1.51 ppm (s, 9 H; C_{17}H). $^{13}\text{C}\{^1\text{H}\}$ NMR (CDCl_3 , 75 MHz, 25 °C): δ 176.7 (C_{14}), 173.1 (C_{12}), 153.6 (C_6), 150.2 (C_2), 137.9 (C_4), 137.3 (C_{4a}), 132.5 (C_{4b}), 131.3 (C_8), 129.0 (C_7), 127.9 (C_9), 126.5 (C_{6a}), 124.9 (C_3), 124.7 (C_{6b}), 122.0 (C_{10}), 118.3 (C_1), 99.0 (C_{13}), 35.5 (C_{16}), 31.5 (C_{17}), 23.1 (C_{15}), 21.8 ppm (C_{11}). ^{19}F NMR (CDCl_3 , 282 MHz, 25 °C): δ -130.7 (dq, $^2J_{\text{FF}} = 96$, $^1J_{\text{FB}} = 18$ Hz, 1F; BF^1), -138.4 ppm (dq, $^2J_{\text{FF}} = 96$, $J_{\text{FB}} = 11$ Hz, 1F; BF^2). ^{11}B NMR (CDCl_3 , 160 MHz, 25 °C): δ 1.0 ppm (dd, $^1J_{\text{BF}} = 12$, 19 Hz). IR (ATR): ν 3100-2800 (C-H stretch, b, w), 1617 ($\text{C}_{14}=\text{N}$ stretch, n, m), 1537 ($\text{C}_{15}=\text{C}_{16}$ stretch, n, m), 1403 ($\text{C}_{16}-\text{O}$ stretch, n, m), 1328 ($\text{C}_{13}-\text{H}$ and $\text{C}_{17}-\text{H}$ bend, n, m), 1261 cm^{-1} (B-F stretch, C_6-H and C_3-H bend, n, m). HRMS (APCI-TOF) m/z : $[\text{M} + \text{H}]^+$ calcd for $[\text{C}_{22}\text{H}_{24}\text{N}_2\text{OBF}_2]^+$ 381.1948; Found 381.1969.

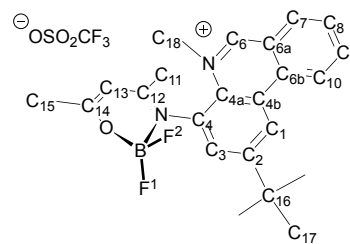
Complex 4: Triethylamine (125 μL , 0.900 mmol) was added to a stirring solution of **L4** (0.100 g, 290 μmol) and boron trifluoride diethyl etherate (183 μL , 1.48 mmol) in toluene (9 mL) heated to reflux in an oil bath set to 110°C for 16 h. A



spectroscopically pure orange solid was isolated. Isolated yield = 98 mg (86%). ^1H NMR (CDCl_3 , 300 MHz, 25 °C): δ 9.32 (s, 1 H; C_6H), 8.83 (s, 1 H; C_1H), 8.56 (d, $^3J_{\text{HH}} = 8.3$ Hz, 1 H; C_{10}H), 8.03 (overlapped m, 2 H; C_3H and C_7H), 7.89 (m, 1 H; C_8H), 7.74 (m, 1 H; C_9H), 5.70 (s, 1 H; C_{13}H), 2.26 (s, 3 H; C_{15}H), 1.87 ppm (s, 3 H; C_{11}H). $^{13}\text{C}\{^1\text{H}\}$ NMR (CDCl_3 , 75 MHz, 25 °C): δ 178.0 (C_{14}), 173.5 (C_{12}), 156.4 (C_6), 141.2 (C_4), 138.7 (C_2),

138.0 (C_{6a}), 132.3 (C_8), 132.0 (C_{4a}), 129.2 (C_7), 129.1 (C_9), 129.1 (C_{4b}) 126.5 (C_{6b}), 122.8 (q, $^4J_{CF} = 3.2$ Hz; C_3), 122.1 (C_{10}), 120.4 (q, $^4J_{CF} = 4.1$ Hz; C_1), 99.2 (C_{13}), 23.2 (C_{11}), 21.8 ppm (C_{15}). ^{19}F NMR (CDCl_3 , 282 MHz, 25 °C): δ -61.7 (s, 3F; $C_{11}\text{F}^3$), -129.8 (dq, $^2J_{FF} = 94$, $^1J_{FB} = 19$ Hz, 1F; BF^1), -138.1 ppm (dq, $^2J_{FF} = 95$, $^1J_{FB} = 11$ Hz, 1F; BF^2). ^{11}B NMR (CDCl_3 , 160 MHz, 25 °C): δ 1.0 ppm (dd, $^1J_{BF} = 12$, 19 Hz). ν 3100-2800 (C-H stretch, b, w), 1616 ($C_{14}=\text{N}$ stretch, n, m), 1538 ($C_{15}=\text{C}_{16}$ stretch, n, m), 1524 cm^{-1} ($C_{16}-\text{O}$ stretch, n, m). HRMS (APCI-TOF) m/z : $[\text{M} + \text{H}]^+$ calcd for $[\text{C}_{19}\text{H}_{15}\text{N}_2\text{OBF}_5]^+$ 393.1196; Found 393.1213.

[3Me]OTf: Methyl trifluoromethanesulfonate (10.0 μL , 88.4 μmol) was added to a stirring solution of **3** (0.0305 g, 80.2 μmol) in CH_2Cl_2 (3 mL) at room temperature. After overnight stirring, the solvent was evaporated, and the brown residue was



subjected to repeated recrystallization (3x) via vapor diffusion of pentane into a CHCl_3 solution to afford a spectroscopically pure product. Beige crystalline solid. Yield = 0.0119 g (27%). ^1H NMR (CDCl_3 , 300 MHz, 25 °C): δ 10.01 (s, 1H; $C_6\text{H}$), 8.84 (d, $^4J_{\text{HH}} = 2.3$ Hz, 1H; $C_1\text{H}$), 8.79 (d, $^3J_{\text{HH}} = 8.4$ Hz, 1H; $C_{10}\text{H}$), 8.60 (d, $^3J_{\text{HH}} = 8.4$ Hz, 1H; $C_7\text{H}$), 8.31 (ddd, $^3J_{\text{HH}} = 8.8$, 7.6 Hz, $^4J_{\text{HH}} = 1.4$ Hz, 1H; $C_9\text{H}$), 8.00 (m, 1H; $C_8\text{H}$), 7.92 (s, 1H; $C_3\text{H}$), 5.87 (s, 1H; $C_{13}\text{H}$), 4.63 (s, 3H; $C_{18}\text{H}$), 2.35 (s, 3H; $C_{11}\text{H}$), 2.03 (s, 3H; $C_{15}\text{H}$), 1.53 ppm (s, 9H; $C_{17}\text{H}$). $^{13}\text{C}\{^1\text{H}\}$ NMR (CDCl_3 , 125 MHz, 25 °C): δ 181.7 (C_{14}), 175.1 (C_{12}), 159.1 (C_6), 154.5 (C_2), 138.7 (C_9), 135.1 (C_{4a}), 133.9 (C_7), 132.0 (C_3), 131.7 (C_{4b}), 131.0 (C_8), 128.9 (C_4), 128.3 (C_{6b}), 124.2 (C_{6a}), 122.7 (C_{10}), 120.9 (C_1), 100.8 (C_{13}), 51.0 (C_{18}), 31.1 (C_{17}), 23.6 (C_{15}), 22.4 (C_{11}) ppm. ^{19}F NMR (CDCl_3 , 282 MHz, 25 °C): δ -78.4 (s, 3F; SO_3CF_3), -128.5 (dq, $^2J_{FF} = 94$ Hz, $^1J_{FB} = 22$ Hz; 1F; BF^1), -141.8 ppm (d, $^2J_{FF} = 93$ Hz,

$^1J_{\text{FB}} = 10 \text{ Hz}$; 1F ; BF^2). ^{11}B NMR (CDCl_3 , 160 MHz , $25 \text{ }^\circ\text{C}$): δ 0.9 ppm (d, $^1J_{\text{BF}} = 22$, 10 Hz). HRMS (ESI-TOF) m/z : $[\text{M}]^+$ calcd for $[\text{C}_{23}\text{H}_{26}\text{N}_2\text{OBF}_2]^+$ 395.2105 ; Found 395.2120 .

Crystal Structure Data

Crystal structure data for **1** (CCDC 2097101): X-ray quality crystals were grown from vapour diffusion of chloroform with hexanes as the non-solvent. Crystal structure parameters: Orange blocks; $\text{C}_{19}\text{H}_{17}\text{BF}_2\text{N}_2\text{O}$ $338.15 \text{ g mol}^{-1}$, orthorhombic, space group $Fdd2$; $a = 19.2122(6) \text{ \AA}$, $b = 42.8928(13) \text{ \AA}$, $c = 7.8535(3) \text{ \AA}$, $\alpha = \beta = \gamma = 90^\circ$, $V = 6471.8(4) \text{ \AA}^3$; $Z = 16$, $\rho_{\text{calcd}} = 1.388 \text{ g cm}^{-3}$; crystal dimensions $0.480 \times 0.200 \times 0.050 \text{ mm}$; $2\theta_{\text{max}} = 61.128^\circ$; 49800 reflections, 4954 independent ($R_{\text{int}} = 0.0617$), intrinsic phasing; $\mu = 0.101 \text{ mm}^{-1}$, absorption correction semi-empirical from equivalents (SADABS); refinement (against F_o^2) with SHELXTL V6.1, 229 parameters, 1 restraints, $R_1 = 0.0532$ ($I > 2\sigma$) and $wR_2 = 0.1172$ (all data), $\text{Goof} = 1.094$, residual electron density $0.25/-0.26 \text{ \AA}^{-3}$.

Crystal structure data for **2** (CCDC 2097102): X-ray quality crystals were grown from vapour diffusion of chloroform and hexanes. Crystal structure parameters: Orange plates; $\text{C}_{20}\text{H}_{19}\text{BF}_2\text{N}_2\text{O}$ $352.18 \text{ g mol}^{-1}$, orthorhombic, space group $Fdd2$; $a = 20.9666(9) \text{ \AA}$, $b = 43.2401(18) \text{ \AA}$, $c = 7.8041(3) \text{ \AA}$, $\alpha = \beta = \gamma = 90^\circ$, $V = 7075.2(5) \text{ \AA}^3$; $Z = 16$, $\rho_{\text{calcd}} = 1.323 \text{ g cm}^{-3}$; crystal dimensions $0.440 \times 0.110 \times 0.030 \text{ mm}$; $2\theta_{\text{max}} = 55.392^\circ$; 48959 reflections, 4144 independent ($R_{\text{int}} = 0.0728$), intrinsic phasing; $\mu = 0.096 \text{ mm}^{-1}$, absorption correction semi-empirical from equivalents (SADABS); refinement (against F_o^2) with SHELXTL V6.1, 239 parameters, 1 restraints, $R_1 = 0.0431$ ($I > 2\sigma$) and $wR_2 = 0.0929$ (all data), $\text{Goof} = 1.059$, residual electron density $0.19/-0.22 \text{ \AA}^{-3}$.

Crystal structure data for **4** (CCDC 2097104): X-ray quality crystals were grown from vapour diffusion of chloroform and hexanes. Crystal structure parameters: Orange blocks; $C_{19}H_{14}BF_5N_2O$ 392.13 g mol⁻¹, monoclinic, space group $P2_1/c$; $a = 10.3312(3)$ Å, $b = 12.1157(4)$ Å, $c = 13.6022(4)$ Å, $\alpha = \gamma = 90^\circ$, $\beta = 90.3410(10)^\circ$, $V = 1702.55(9)$ Å³; $Z = 4$, $\rho_{\text{calcd}} = 1.530$ g cm⁻³; crystal dimensions 0.470 x 0.410 x 0.250 mm; $2\theta_{\text{max}} = 72.786^\circ$; 74965 reflections, 8277 independent ($R_{\text{int}} = 0.0578$), intrinsic phasing; $\mu = 0.132$ mm⁻¹, absorption correction semi-empirical from equivalents (SADABS); refinement (against F_o^2) with SHELXTL V6.1, 255 parameters, 0 restraints, $R_1 = 0.0696$ ($I > 2\sigma$) and $wR_2 = 0.1786$ (all data), Goof = 1.045, residual electron density 0.51/-0.37 Å⁻³.

Crystal structure data for [3Me]OTf (CCDC 2097103): X-ray quality crystals were grown from vapour diffusion of pentane into a chloroform solution. Crystal structure parameters: Colourless needles; $C_{25}H_{27}BCl_3F_5N_2O_4S$ 663.70 g mol⁻¹, monoclinic, space group $P2_1/n$; $a = 14.6473(8)$ Å, $b = 7.2455(4)$ Å, $c = 28.3346(15)$ Å, $\alpha = \gamma = 90^\circ$, $\beta = 97.785(2)^\circ$, $V = 2979.4(3)$ Å³; $Z = 4$, $\rho_{\text{calcd}} = 1.480$ g cm⁻³; crystal dimensions 0.80 x 0.20 x 0.07 mm; $2\theta_{\text{max}} = 52.730^\circ$; 64607 reflections, 6051 independent ($R_{\text{int}} = 0.0598$), intrinsic phasing; $\mu = 0.444$ mm⁻¹, absorption correction semi-empirical from equivalents (SADABS); refinement (against F_o^2) with SHELXTL V6.1, 376 parameters, 0 restraints, $R_1 = 0.0799$ ($I > 2\sigma$) and $wR_2 = 0.2174$ (all data), Goof = 1.052, residual electron density 1.919/-0.548 Å⁻³.

UV-Vis Absorption and Luminescence Measurements. Absorption spectra were measured on a Biotek Instruments XS spectrometer, using quartz cuvettes of 1 cm pathlength. Steady-state luminescence spectra were measured using a Jobin Yvon

FluoroMax-2 spectrofluorimeter, fitted with a red-sensitive Hamamatsu R928 photomultiplier tube; the spectra shown are corrected for the wavelength dependence of the detector, and the quoted emission maxima refer to the values after correction. Degassed samples for emission measurements were contained within quartz cuvettes of 1 cm pathlength modified with appropriate glassware to allow connection to a high-vacuum line. Degassing was achieved via a minimum of three freeze-pump-thaw cycles whilst connected to the vacuum manifold. Luminescence quantum yields were determined using quinine sulfate in 1M H₂SO₄(aq) as the standard ($\Phi = 0.546$).⁵³ Fluorescence lifetimes were measured, where possible, by time-correlated single-photon counting following excitation at 374 nm with a pulsed-diode laser. The emitted light was detected at 90° using a Peltier-cooled R928 PMT after passage through a monochromator. Phosphorescence lifetimes at 77 K were measured following excitation with a microsecond-pulsed xenon lamp and detection using the same PMT operating in multichannel scaling mode.

Computational Details. Optimizations and PES scans were performed using Gaussian 16 Rev.C01⁵⁴, while single points were carried out using Orca ver. 4.2.1.⁵⁵ Restricted and unrestricted Kohn-Sham density functional theory (DFT) were carried out on close-shell (¹S_{0,eq}) and open-shell species (³T_{1,eq}), respectively. The ground state and lowest excited triplet state geometries of **1-4** and [3Me]⁺ were carried out both in gas and solution phases (SMD⁵⁶ = CH₂Cl₂) using the CAM-B3LYP functional⁵⁷ in combination with Grimme's dispersion correction with Becke-Johnson damping (D3BJ)⁵⁸ and Ahlrichs double- ζ basis with polarization on non-hydrogen atoms, def2-SV(P)⁵⁹. The absence of imaginary frequencies confirmed that the optimized geometries were at minima. The potential energy

surface of **3** in gas and solution phases (SMD = CH₂Cl₂) were scanned along the oxazaborinine-phenanthridinyl dihedral allowing nuclear relaxation after each rotation employing CAM-B3LYP-D3(BJ)/def2-SV(P). Single point calculations including time-dependent DFT (TDDFT) were carried out using M062X⁶⁰ with Ahlrichs triple- ζ basis with reduced polarization on hydrogen atom, def2-TZVP(-f)⁵⁹. The resolution of identity with chains of spheres approximation and def2/J⁶¹ auxiliary basis sets were implemented to speed up single-point and TDDFT calculations. DFT integration grids were set to Grid5 and Finalgrid6, while the COSX integration grids were set to intaccx: 4.34, 4.34, 4.67 and gridx 2,2,2. SCF and energy convergence criteria were set to tightscf. Molecular orbital isosurfaces were generated using Avogadro,⁶² while spin densities of the lowest-lying excited triplet states were generated using Gabedit.⁶³ Orbital and electronic excitation⁶⁴ analyses were carried out using Multiwfn v.3.7.⁶⁵ PESs were generated using Gaussview 6.⁶⁶

ASSOCIATED CONTENT

Supporting Information. Packing diagrams; additional UV-Vis absorption and emission spectra; computational data tables; multi-nuclear NMR spectra of all new compounds; crystallographic information files containing all X-ray data. CCDC 2097101-2097104 contain the supplementary crystallographic data for this paper. The data can be obtained free of charge from The Cambridge Crystallographic Data Center via www.ccdc.cam.ac.uk/structures.

The following files are available free of charge:

Supporting Information File (PDF)

Combined Crystallographic Information File (CIF)

AUTHOR INFORMATION

Corresponding Author

David E. Herbert (david.herbert@umanitoba.ca)

ORCID^s

Issiah B. Lozada: 0000-0002-1689-2918

Robert J. Ortiz: 0000-0001-9078-765X

Jason D. Braun: 0000-0002-5850-8048

J. A. Gareth Williams: 0000-0002-4688-3000

David E. Herbert: 0000-0001-8190-2468

Author Contributions

The manuscript was written through contributions of all authors. All authors have given approval to the final version of the manuscript.

Conflicts of Interest

There are no conflicts of interest to declare.

ACKNOWLEDGEMENTS

The following sources of funding are gratefully acknowledged: the Natural Sciences Engineering Research Council of Canada for a Discovery Grant to DEH (RGPIN-2014-03733); the Canadian Foundation for Innovation and Research Manitoba for an award in support of an X-ray diffractometer (CFI #32146); Compute Canada for access to computational resources; and the University of Manitoba for UMGF Fellowships (RJO, JDB), the Bert & Lee Friesen Graduate Scholarship (IBL) and GETS support.

REFERENCES

- (1) Turksoy, A.; Yildiz, D.; Akkaya, E. U. Photosensitization and Controlled Photosensitization with BODIPY Dyes. *Coord. Chem. Rev.* **2019**, *379*, 47–64.
- (2) Poddar, M.; Misra, R. Recent Advances of BODIPY Based Derivatives for Optoelectronic Applications. *Coord. Chem. Rev.* **2020**, *421*, 213462.
- (3) Møllerup, S. K.; Wang, S. Boron-Based Stimuli Responsive Materials. *Chem. Soc. Rev.* **2019**, *48*, 3537–3549.
- (4) Kamkaew, A.; Lim, S. H.; Lee, H. B.; Kiew, L. V.; Chung, L. Y.; Burgess, K. BODIPY Dyes in Photodynamic Therapy. *Chem. Soc. Rev.* **2013**, *42*, 77–88.
- (5) Kowada, T.; Maeda, H.; Kikuchi, K. BODIPY-Based Probes for the Fluorescence Imaging of Biomolecules in Living Cells. *Chem. Soc. Rev.* **2015**, *44*, 4953–4972.
- (6) Bertrand, B.; Passador, K.; Goze, C.; Denat, F.; Bodio, E.; Salmain, M. Metal-Based BODIPY Derivatives as Multimodal Tools for Life Sciences. *Coord. Chem. Rev.* **2018**, *358*, 108–124.
- (7) Loudet, A.; Burgess, K. BODIPY Dyes and Their Derivatives: Syntheses and Spectroscopic Properties. *Chem. Rev.* **2007**, *107*, 4891–4932.
- (8) Boens, N.; Verbelen, B.; Ortiz, M. J.; Jiao, L.; Dehaen, W. Synthesis of BODIPY Dyes through Postfunctionalization of the Boron Dipyrromethene Core. *Coord. Chem. Rev.* **2019**, *399*, 213024.
- (9) Macedo, F. P.; Gwengo, C.; Lindeman, S. V.; Smith, M. D.; Gardinier, J. R. β -Diketonate, β -Ketoiminate, and β -Diiminate Complexes of Difluoroboron. *Eur. J. Inorg. Chem.* **2008**, *2008*, 3200–3211.
- (10) Yoshii, R.; Hirose, A.; Tanaka, K.; Chujo, Y. Functionalization of Boron Diiminates with Unique Optical Properties: Multicolor Tuning of Crystallization-Induced Emission and Introduction into the Main Chain of Conjugated Polymers. *J. Am. Chem. Soc.* **2014**, *136*, 18131–18139.
- (11) Yoshii, R.; Hirose, A.; Tanaka, K.; Chujo, Y. Boron Diiminate with Aggregation-Induced Emission and Crystallization-Induced Emission-Enhancement Characteristics. *Chem. - Eur. J.* **2014**, *20*, 8320–8324.
- (12) Chen, P.-Z.; Niu, L.-Y.; Chen, Y.-Z.; Yang, Q.-Z. Difluoroboron β -Diketonate Dyes: Spectroscopic Properties and Applications. *Coord. Chem. Rev.* **2017**, *350*, 196–216.
- (13) Wang, J.-X.; Yu, Y.-S.; Niu, L.-Y.; Zou, B.; Wang, K.; Yang, Q.-Z. A Difluoroboron β -Diketonate Based Thermometer with Temperature-Dependent Emission Wavelength. *Chem. Commun.* **2020**, *56*, 6269–6272.
- (14) Itoh, K.; Okazaki, K.; Sera, A.; Chow, Y. L. The Photoaddition of Enaminoketonatoboron Difluorides with Trans-Stilbene. *J. Chem. Soc. Chem. Commun.* **1992**, 1608–1609.
- (15) Itoh, K.; Fujimoto, M.; Hashimoto, M. Photodimerization of Enaminoketonatoboron Difluorides. *New J. Chem.* **2002**, *26*, 1070–1075.
- (16) Itoh, K.; Okazaki, K.; Chow, Y. L. Photocycloaddition of Some Difluoro(Aminoenoato)Boron Complexes with Arylalkenes. *Helv. Chim. Acta* **2004**, *87*, 292–302.
- (17) Graser, M.; Kopacka, H.; Wurst, K.; Ruetz, M.; Kreutz, C. R.; Müller, T.; Hirtenlehner, C.; Monkowius, U.; Knor, G.; Bildstein, B. Efficient Fluorophores

- Based on Pyridyl-Enolato and Enamido Difluoroboron Complexes: Simple Alternatives to Boron-Dipyrrromethene (Bodipy) Dyes. *Inorganica Chim. Acta* **2013**, *405*, 116–120.
- (18) Dohe, J.; Kossmann, J.; Mueller, T. J. J. Diversity-Oriented Four-Component Synthesis of Solid State Luminescent Difluoro Oxazaborinines. *Dyes Pigments* **2018**, *157*, 198–217.
- (19) Grabarz, A. M.; Jedrzejewska, B.; Zakrzewska, A.; Zalesny, R.; Laurent, A. D.; Jacquemin, D.; Osmialowski, B. Photophysical Properties of Phenacylphenanthridine Difluoroboranyl: Effect of Substituent and Double Benzannulation. *J. Org. Chem.* **2017**, *82*, 1529–1537.
- (20) Frath, D.; Azizi, S.; Ulrich, G.; Retailleau, P.; Ziessel, R. Facile Synthesis of Highly Fluorescent Boranil Complexes. *Org. Lett.* **2011**, *13*, 3414–3417.
- (21) Shanmugapriya, J.; Rajaguru, K.; Sivaraman, G.; Muthusubramanian, S.; Bhuvanesh, N. Boranil Dye Based “Turn-on” Fluorescent Probes for Detection of Hydrogen Peroxide and Their Cell Imaging Application. *RSC Adv.* **2016**, *6*, 85838–85843.
- (22) Zhao, N.; Ma, C.; Yang, W.; Yin, W.; Wei, J.; Li, N. Facile Construction of Boranil Complexes with Aggregation-Induced Emission Characteristics and Their Specific Lipid Droplet Imaging Applications. *Chem. Commun.* **2019**, *55*, 8494–8497.
- (23) Zhu, D.; Yan, X.; Ren, A.; Cai, W.; Duan, Z.; Luo, Y. Modulation of ICT and PET Processes in Boranil Derivatives: A Ratiometric Fluorescent Probe for Imaging of Cysteine. *Anal. Methods* **2019**, *11*, 2579–2584.
- (24) Le Guennic, B.; Chibani, S.; Charaf-Eddin, A.; Massue, J.; Ziessel, R.; Ulrich, G.; Jacquemin, D. The NBO Pattern in Luminescent Chromophores: Unraveling Excited-State Features Using TD-DFT. *Phys. Chem. Chem. Phys.* **2013**, *15*, 7534–7540.
- (25) Lozada, I. B.; Huang, B.; Stilgenbauer, M.; Beach, T.; Qiu, Z.; Zheng, Y.; Herbert, D. E. Monofunctional Platinum(II) Anticancer Complexes Based on Multidentate Phenanthridine-Containing Ligand Frameworks. *Dalton Trans.* **2020**, *49*, 6557–6560.
- (26) Mandapati, P.; Giesbrecht, P. K.; Davis, R. L.; Herbert, D. E. Phenanthridine-Containing Pincer-like Amido Complexes of Nickel, Palladium, and Platinum. *Inorg. Chem.* **2017**, *56*, 3674–3685.
- (27) Mondal, R.; Lozada, I. B.; Davis, R. L.; Williams, J. A. G.; Herbert, D. E. Exploiting Synergy between Ligand Design and Counterion Interactions to Boost Room Temperature Phosphorescence from Cu(I) Compounds. *J. Mater. Chem. C* **2019**, *7*, 3772–3778.
- (28) Mandapati, P.; Braun, J. D.; Lozada, I. B.; Williams, J. A. G.; Herbert, D. E. Deep-Red Luminescence from Platinum(II) Complexes of N[^]N[^]N-Amido Ligands with Benzannulated N-Heterocyclic Donor Arms. *Inorg. Chem.* **2020**, *59*, 12504–12517.
- (29) Myers, E. L.; Butts, C. P.; Aggarwal, V. K. BF₃·OEt₂ and TMSOTf: A Synergistic Combination of Lewis Acids. *Chem. Commun.* **2006**, No. 42, 4434–4436.
- (30) Köhling, J.; Kozel, V.; Jovanov, V.; Pajkert, R.; Tverdomed, S. N.; Gridenco, O.; Fugel, M.; Grabowsky, S.; Rösenthaller, G.-V.; Wagner, V. Synthesis and Characterization of Oxazaborinin Phosphonate for Blue OLED Emitter Applications. *ChemPhysChem* **2019**, *20*, 665–671.

- (31) Mtiraoui, H.; Gharbi, R.; Msaddek, M.; Bretonnière, Y.; Andraud, C.; Renard, P.-Y.; Sabot, C. Solution and Solid-State Fluorescence of 2-(2'-Hydroxyphenyl)-1,5-Benzodiazepin-2-One (HBD) Borate Complexes. *RSC Adv.* **2016**, *6*, 86352–86360.
- (32) Chęcińska, L.; Mebs, S.; Ośmiałowski, B.; Zakrzewska, A.; Ejsmont, K.; Kohout, M. Tuning the Electronic Properties of the Dative N–B Bond with Associated O–B Interaction: Electron Localizability Indicator from X-Ray Wavefunction Refinement. *ChemPhysChem* **2016**, *17*, 2395–2406.
- (33) Itoh, K.; Okazaki, K.; Fujimoto, M. The Structure of 1,3-Enaminoketonatoboron Difluorides in Solution and in the Solid State. *Aust. J. Chem.* **2003**, *56*, 1209–1214.
- (34) Grepioni, F.; Cojazzi, G.; Draper, S. M.; Scully, N.; Braga, D. Crystal Forms of Hexafluorophosphate Organometallic Salts and the Importance of Charge-Assisted C–H...F Hydrogen Bonds. *Organometallics* **1998**, *17*, 296–307.
- (35) Mandapati, P.; Braun, J. D.; Killeen, C.; Davis, R. L.; Williams, J. A. G.; Herbert, D. E. Luminescent Platinum(II) Complexes of N^N-Amido Ligands with Benzannulated N-Heterocyclic Donor Arms: Quinolines Offer Unexpectedly Deeper Red Phosphorescence than Phenanthridines. *Inorg. Chem.* **2019**, *58*, 14808–14817.
- (36) Lozada, I. B.; Williams, J. A. G.; Herbert, D. E. Platinum(II) Complexes of Benzannulated N^N-O-Amido Ligands: Bright Orange Phosphors with Long-Lived Excited States. *Inorg. Chem. Front.* **2021**. <https://doi.org/10.1039/D1QI01120K>.
- (37) Donckt, E. V.; Dramaix, R.; Nasielski, J.; Vogels, C. Photochemistry of Aromatic Compounds. Part 1.—Acid-Base Properties of Singlet and Triplet Excited States of Pyrene Derivatives and Aza-Aromatic Compounds. *Trans. Faraday Soc.* **1969**, *65*, 3258–3262.
- (38) Zander, M. The Significance of Donor-Acceptor Interactions in the External Heavy Atom Effect of Silver Nitrate on the Luminescence Behavior of Aza-Aromatic Systems and Carbazoles. *Z Naturforsch A* **1978**, *33*, 998–1000.
- (39) Norek, M.; Dresner, J.; Prochorow, J. Spectroscopy and Photophysics of Monoazaphenanthrenes. I. Absorption and Fluorescence Spectra of Phenanthridine and 7,8-Benzoquinoline. *Acta Phys. Pol. A* **2003**, *104*, 425–439.
- (40) Marzacco, C. J.; Deckey, G.; Colarulli, R.; Siuzdak, G.; Halpern, A. M. Excited-State Protonation and Photophysical Properties of Azaphenanthrenes. *J. Phys. Chem.* **1989**, *93*, 2935–2939.
- (41) Parker, D.; Senanayake, P. K.; Williams, J. A. G. Luminescent Sensors for PH, PO₂, Halide and Hydroxide Ions Using Phenanthridine as a Photosensitiser in Macrocyclic Europium and Terbium Complexes. *J. Chem. Soc. Perkin Trans. 2* **1998**, 2129–2140.
- (42) Norek, M.; Kozankiewicz, B.; Prochorow, J. Spectroscopy and Photophysics of Monoazaphenanthrenes. III. Luminescence of Phenanthridine and 7,8-Benzoquinoline in Crystalline State. *Acta Phys Pol A* **2004**, *106*, 77–94.
- (43) Chibani, S.; Charaf-Eddin, A.; Le Guennic, B.; Jacquemin, D. Boranil and Related NBO Dyes: Insights From Theory. *J. Chem. Theory Comput.* **2013**, *9*, 3127–3135.
- (44) Tomasi, J.; Mennucci, B.; Cammi, R. Quantum Mechanical Continuum Solvation Models. *Chem Rev* **2005**, *105*, 2999–3094.

- (45) Mondal, R.; Giesbrecht, P. K.; Herbert, D. E. Nickel(II), Copper(I) and Zinc(II) Complexes Supported by a (4-Diphenylphosphino)Phenanthridine Ligand. *Polyhedron* **2016**, *108*, 156–162.
- (46) Mondal, R.; Lozada, I. B.; Davis, R. L.; Williams, J. A. G.; Herbert, D. E. Site-Selective Benzannulation of N-Heterocycles in Bidentate Ligands Leads to Blue-Shifted Emission from $[(P^N)Cu]_2(\mu-X)_2$ Dimers. *Inorg Chem* **2018**, *57*, 4966–4978.
- (47) Gaire, S.; Ortiz, R. J.; Schrage, B. R.; Lozada, I. B.; Mandapati, P.; Osinski, A. J.; Herbert, D. E.; Ziegler, C. J. (8-Amino)Quinoline and (4-Amino)Phenanthridine Complexes of $Re(CO)_3$ Halides. *J. Organomet. Chem.* **2020**, *921*, 121338.
- (48) Melenbacher, A.; Dhindsa, J. S.; Gilroy, J. B.; Stillman, M. J. Unveiling the Hidden, Dark, and Short Life of a Vibronic State in a Boron Difluoride Formazanate Dye. *Angew. Chem. Int. Ed.* **2019**, *58* (43), 15339–15343.
- (49) El-Sayed, M. A. Spin—Orbit Coupling and the Radiationless Processes in Nitrogen Heterocyclics. *J. Chem. Phys.* **1963**, *38* (12), 2834–2838.
- (50) Bruker-AXS. *APEX3 V2016.1-0*; Madison, Wisconsin, USA, 2016.
- (51) Dolomanov, O. V.; Bourhis, L. J.; Gildea, R. J.; Howard, J. A. K.; Puschmann, H. OLEX2: A Complete Structure Solution, Refinement and Analysis Program. *J. Appl. Crystallogr.* **2009**, *42*, 339–341.
- (52) Spek, A. L. Structure Validation in Chemical Crystallography. *Acta Cryst* **2009**, *D65*, 148–155.
- (53) Meech, S. R.; Phillips, D. Photophysics of Some Common Fluorescence Standards. *J. Photochem.* **1983**, *23*, 193–217.
- (54) Frisch, M. J.; Trucks, G. W.; Schlegel, H. B.; Scuseria, G. E.; Robb, M. A.; Cheeseman, J. R.; Scalmani, G.; Barone, V.; Petersson, G. A.; Nakatsuji, H.; Li, X.; Caricato, M.; Marenich, A. V.; Bloino, J.; Janesko, B. G.; Gomperts, R.; Mennucci, B.; Hratchian, H. P.; Ortiz, J. V.; Izmaylov, A. F.; Sonnenberg, J. L.; Williams; Ding, F.; Lipparini, F.; Egidi, F.; Goings, J.; Peng, B.; Petrone, A.; Henderson, T.; Ranasinghe, D.; Zakrzewski, V. G.; Gao, J.; Rega, N.; Zheng, G.; Liang, W.; Hada, M.; Ehara, M.; Toyota, K.; Fukuda, R.; Hasegawa, J.; Ishida, M.; Nakajima, T.; Honda, Y.; Kitao, O.; Nakai, H.; Vreven, T.; Throssell, K.; Montgomery Jr., J. A.; Peralta, J. E.; Ogliaro, F.; Bearpark, M. J.; Heyd, J. J.; Brothers, E. N.; Kudin, K. N.; Staroverov, V. N.; Keith, T. A.; Kobayashi, R.; Normand, J.; Raghavachari, K.; Rendell, A. P.; Burant, J. C.; Iyengar, S. S.; Tomasi, J.; Cossi, M.; Millam, J. M.; Klene, M.; Adamo, C.; Cammi, R.; Ochterski, J. W.; Martin, R. L.; Morokuma, K.; Farkas, O.; Foresman, J. B.; Fox, D. J. *Gaussian 16 Rev. C.01*; Wallingford, CT, 2016.
- (55) Neese, F. Software Update: The ORCA Program System, Version 4.0. *WIREs Comput. Mol. Sci.* **2018**, *8*, e1327.
- (56) Marenich, A. V.; Cramer, C. J.; Truhlar, D. G. Universal Solvation Model Based on Solute Electron Density and on a Continuum Model of the Solvent Defined by the Bulk Dielectric Constant and Atomic Surface Tensions. *J Phys Chem B* **2009**, *113*, 6378–6396.
- (57) Yanai, T.; Tew, D. P.; Handy, N. C. A New Hybrid Exchange–Correlation Functional Using the Coulomb-Attenuating Method (CAM-B3LYP). *Chem. Phys. Lett.* **2004**, *393*, 51–57.

- (58) Grimme, S.; Ehrlich, S.; Goerigk, L. Effect of the Damping Function in Dispersion Corrected Density Functional Theory. *J. Comput. Chem.* **2011**, *32*, 1456–1465.
- (59) Weigend, F.; Ahlrichs, R. Balanced Basis Sets of Split Valence, Triple Zeta Valence and Quadruple Zeta Valence Quality for H to Rn: Design and Assessment of Accuracy. *Phys. Chem. Chem. Phys.* **2005**, *7*, 3297.
- (60) Zhao, Y.; Truhlar, D. G. The M06 Suite of Density Functionals for Main Group Thermochemistry, Thermochemical Kinetics, Noncovalent Interactions, Excited States, and Transition Elements: Two New Functionals and Systematic Testing of Four M06-Class Functionals and 12 Other Functionals. *Theor. Chem. Acc.* **2008**, *120*, 215–241.
- (61) Weigend, F. Accurate Coulomb-Fitting Basis Sets for H to Rn. *Phys. Chem. Chem. Phys.* **2006**, *8*, 1057.
- (62) Hanwell, M. D.; Curtis, D. E.; Lonie, D. C.; Vandermeersch, T.; Zurek, E.; Hutchison, G. R. Avogadro: An Advanced Semantic Chemical Editor, Visualization, and Analysis Platform. *J Cheminf* **2012**, *4*, 17.
- (63) Allouche, A.-R. Gabedit—A Graphical User Interface for Computational Chemistry Softwares. *J. Comput. Chem.* **2011**, *32*, 174–182.
- (64) Liu, Z.; Lu, T.; Chen, Q. An Sp-Hybridized All-Carboatomic Ring, Cyclo[18]Carbon: Electronic Structure, Electronic Spectrum, and Optical Nonlinearity. *Carbon* **2020**, *165*, 461–467.
- (65) Lu, T.; Chen, F. Multiwfn: A Multifunctional Wavefunction Analyzer. *J Comput Chem* **2012**, *33*, 580–592.
- (66) Dennington, Roy; Keith, Todd A.; Millam, John M. *GaussView, Version 6*; Semichem Inc.: Shawnee Mission, KS, 2016.

Table of Contents Graphic

